

1 **Jurassic–Paleogene Intra–Oceanic Magmatic Evolution of the Ankara Mélange, North–**
2 **Central Anatolia, Turkey**

3 Ender Sarifakioglu¹, Yildirim Dilek² and Mustafa Sevin¹

4 ¹General Directorate of Mineral Research & Exploration, Department of Geology, TR–06520
5 Ankara, Turkey, esarifakioglu@mta.gov.tr

6 ²Department of Geology & Env. Earth Science, Miami University, Oxford, OH 45056, USA,
7 dileky@miamioh.edu

8
9 **Abstract**

10 Oceanic rocks in the Ankara Mélange along the Izmir–Ankara–Erzincan suture zone (IAESZ)
11 in North–Central Anatolia include locally coherent ophiolite complexes (~179 Ma and ~80
12 Ma), seamount or oceanic plateau volcanic units with pelagic and reefal limestones (96.6±1.8
13 Ma), metamorphic rocks with ages of 187.4±3.7 Ma, 158.4±4.2 Ma, and 83.5±1.2 Ma, and
14 subalkaline to alkaline volcanic and plutonic rocks of an island arc origin (~67–63 Ma). All but
15 the arc rocks occur in a shaly–graywacke and/or serpentinite matrix, and are deformed by
16 south–vergent thrust faults and folds that developed in the Middle to Late Eocene due to
17 continental collisions in the region. Ophiolitic volcanic rocks have mid–ocean ridge (MORB)
18 and island arc tholeiite (IAT) affinities showing moderate to significant large ion lithophile
19 elements (LILE) enrichment and depletion in Nb, Hf, Ti, Y and Yb, which indicate the
20 influence of subduction–derived fluids in their melt evolution. Seamount/oceanic plateau
21 basalts show ocean island basalt (OIB) affinities. The arc–related volcanic rocks,
22 lamprophyric dikes and syeno–dioritic plutons exhibit high–K shoshonitic to medium–to high–
23 K calc–alkaline compositions with strong enrichment in LILE, rare earth elements (REE) and
24 Pb, and initial ε_{Nd} values between +1.3 and +1.7. Subalkaline arc volcanic units occur in the
25 northern part of the mélange, whereas the younger alkaline volcanic rocks and intrusions
26 (lamprophyre dikes and syeno–dioritic plutons) in the southern part. The Early to Late
27 Jurassic and Late Cretaceous epidote–actinolite, epidote–chlorite and epidote–glaucophane
28 schists represent the metamorphic units formed in a subduction channel in the Northern
29 Neotethys. The Middle to Upper Triassic neritic limestones spatially associated with the
30 seamount volcanic rocks indicate that the Northern Neotethys was an open ocean with its
31 MORB–type oceanic lithosphere by the Early Triassic. The Latest Cretaceous–Early
32 Paleocene island arc volcanic, dike and plutonic rocks with subalkaline to alkaline
33 geochemical affinities represent intraoceanic magmatism that developed on and across the
34 subduction–accretion complex above a N–dipping, southward–rolling subducted lithospheric
35 slab within the Northern Neotethys. The Ankara Mélange thus exhibits the record of ~120–
36 130 million years of oceanic magmatism in geological history of the Northern Neotethys.

37
38 **Keywords:** Ankara Mélange (Turkey), Northern Neotethys, seamount volcanics,
39 suprasubduction zone ophiolites, subduction–accretion complex, island arc magmatism

41 **1. Introduction**

42 In this paper we document the internal structure of the Ankara Mélange along the IAESZ in
43 North–Central Anatolia, and present new geochemical and geochronological data from
44 various magmatic rock assemblages that make up distinct tectonic units in this mélange. Our
45 geochemical data and interpretations indicate that all units within the Ankara Mélange are
46 intraoceanic in origin and appear to have formed during the seafloor spreading, seamount
47 volcanism and island arc magmatism stages of the Northern Neotethys. We also present
48 new Pb–Sr–Nd isotopic compositional data, and radiometric data belonging to both
49 magmatic arc rocks and basic rocks from the Ankara Mélange. Thus, the Ankara Mélange
50 displays a complete record of ~120–130 m.y. of intraoceanic magmatism that took place prior
51 to the continental collisional events in Anatolia in the Eocene.

52 **2. Regional Geology**

53 The IAESZ forms the tectonic boundary between the Pontide tectonic belt (including the
54 Sakarya Continent) in the north and the Anatolide–Tauride block including the Central
55 Anatolian Crystalline Complex (CACC) in the south. The suture zone is marked by ophiolite
56 units, ophiolitic mélanges, and seamount fragments. The Sakarya Continent in the Pontides
57 represents the southern margin of Eurasia (Figs. 1 and 2). Carboniferous (330–310 Ma),
58 high–grade metamorphic rocks (gneiss, migmatite, amphibolite and marble), currently
59 exposed in the Kazdağ, Söğüt, Devrekani, and Pulur massifs (from west to east), make up
60 the continental basement of the Sakarya Continent (Topuz et al., 2004, 2006; Okay et al.,
61 2006; Nzegge et al., 2006). These metamorphic basement rocks are intruded by the
62 Carboniferous (295 Ma) granitoids (Çoğulu et al., 1965; Delaloye and Bingöl, 2000). The
63 Triassic Karakaya Complex, representing a subduction–accretion complex, tectonically
64 overlies the crystalline basement units (Tekeli, 1981). It includes the Lower Karakaya, which
65 comprises metabasite, marble and phyllite rocks, and the Upper Karakaya consisting mainly
66 of unmetamorphosed clastic and basic volcanic rocks with blocks of Carboniferous and
67 Permian neritic limestones (Bingöl et al., 1975; Okay et al., 2002; Okay and Göncüoğlu,
68 2004).

69 The CACC consists mainly of Paleozoic–Mesozoic metamorphic massifs (Kırşehir, Akdağ,
70 and Niğde massifs) and Cretaceous–Paleocene granitoids (Fig. 2). The metamorphic
71 massifs comprise metacarbonate, metapelite and amphibolite–gneiss rocks that are the
72 products of varied P/T conditions of metamorphism (Whitney and Dilek 1998). The Late
73 Cretaceous granitoids and the Eocene–Upper Miocene volcanic rocks crosscut and overlie

74 (respectively) the crystalline basement units of the CACC (Güleç, 1994; Boztuğ, 2000;
75 Kadioğlu et al., 2003, 2006; İlbeyli et al., 2004). The Late Cretaceous plutons are composed
76 of *Granite*, *Monzonite* and *Syenite Supersuites* with ages of 77.7 ± 0.3 Ma, 70 ± 1.0 Ma and
77 69.8 ± 0.3 Ma, respectively (Kadioğlu et al., 2006). They display a chemical progression from
78 high-K calc-alkaline and high-K shoshonitic to alkaline compositions, representing the
79 development of within-plate magmatism across the CACC with time (Kadioğlu et al., 2006).

80 **3. Internal Structure and Tectonic Units of the Ankara Mélange**

81 The most important component of the IAESZ in its central segment in northern Anatolia is the
82 Ankara Mélange, extending from Ankara in the west to Çorum in the east (Fig. 2). The
83 Ankara Mélange is a well known subduction-accretion complex (Bailey and McCallien, 1950,
84 1953), consisting of blocks of Paleozoic limestone and metamorphic rocks, Jurassic-
85 Cretaceous ophiolitic units, and Jurassic-Cretaceous seamount volcanic assemblages in a
86 shaly-graywacke and/or serpentinite matrix (Figs. 3 and 4; Norman, 1984; Akyürek et al.,
87 1984; Koçyiğit, 1991; Tüysüz et al., 1995; Tankut et al., 1998; Dilek and Thy, 2006;
88 Dangerfield et al., 2011).

89 Megablocks and imbricated thrust sheets of oceanic rocks occur as mappable units
90 enveloped in a pelitic (clayey, sandy-silty), serpentinite or volcanic matrix within the Ankara
91 Mélange (Fig. 5). In some of these blocks or thrust sheets the mafic-ultramafic rock units
92 and the associated sedimentary rocks make up coherent ophiolite complexes (e.g. the
93 Eldivan ophiolite) (Figs. 6 and 7), representing the Neotethyan oceanic lithosphere.
94 Plagiogranite dikes intruding the serpentinitized peridotites near Eldivan (Çankırı) revealed U-
95 Pb zircon ages of 179 Ma (Dilek and Thy, 2006), indicating that part of the Neotethyan
96 oceanic crust preserved in the mélange is as old as the Early Jurassic. The radiolarian fauna
97 in the chert blocks have yielded Late Carnian-Middle Norian, and Middle Jurassic to Middle
98 Cretaceous ages (Sarifikioğlu et al., unpublished data). However, the whole-rock $^{40}\text{Ar}/^{39}\text{Ar}$
99 dating of basaltic pillow lava from an ophiolitic thrust sheet farther south in the Ankara
100 Mélange has revealed an age of 80.3 ± 7.6 Ma, indicating that Late Cretaceous oceanic
101 crustal rocks also exist within the mélange (Table 1).

102 The Senomanian-Santonian flyschoidal sedimentary rocks with pebblestone, sandstone,
103 mudstone and clayey limestone with interbedded chert layers unconformably rest on the
104 ophiolitic rocks (Figs. 3 and 4). However, Kimmeridgian-Hauterivian flyschoidal sedimentary
105 rocks cover the ophiolitic pillow lavas farther south in the Ankara Mélange (Sarifikioğlu et al.,
106 unpublished data). The Upper Santonian-Maastrichtian, thin- to medium-layered clayey to

107 sandy limestone and volcanic detrital rocks rest unconformably on these flyschoidal
108 sedimentary and ophiolitic rocks around Yapraklı (Çankırı) and Laloğlu (Çorum), and
109 represent the forearc basin strata (Figs. 6 and 7). The ophiolitic, flyschoidal and forearc basin
110 rocks are imbricated along south-directed thrust faults (Sarifakioglu et al., 2011).

111 Blocks (km-size) of alkaline volcanic and pyroclastic rocks, debris flow deposits, and
112 coarse-grained reefal limestones representing seamount and/or oceanic plateau fragments
113 also occur in the Ankara Mélange (Fig. 8). We have obtained Middle–Upper Triassic and
114 Cretaceous biostratigraphic ages from the reefal limestones overlying the seamount volcanic
115 units, and $^{40}\text{Ar}/^{39}\text{Ar}$ whole-rock ages of 96.6 ± 1.8 Ma from the alkaline pillow lavas that are
116 stratigraphically associated with the pink colored pelagic limestones (Sarifakioglu et al.,
117 unpublished data). Rojay et al. (2004) obtained the Late Barremian–Early Aptian
118 biostratigraphic ages from the reefal limestones resting on the pillow lavas with ocean island
119 basalt (OIB) geochemical affinities. Blocks of these neritic carbonates and the underlying
120 alkaline pillow lavas are also embedded in a turbiditic sequence consisting of chert and
121 volcanic rock clasts in a fine-grained sandstone matrix. Volcanic debris flow deposits also
122 occur within the turbiditic sequence.

123 In addition to the blocks of ophiolitic, seamount and oceanic plateau rocks, the Ankara
124 Mélange also contains blocks of metamorphic rocks, mainly epidote–glaucophane, epidote–
125 chlorite, and epidote–actinolite schists (Fig. 6). The geochemical fingerprinting of these rocks
126 suggests that their protoliths were made of seamount volcanics and ophiolitic basic rocks,
127 and related sediments. Detailed descriptions and documentation of these metamorphic rocks
128 will be presented elsewhere. We interpret these metamorphic rocks to have formed in an
129 intra-oceanic subduction zone. The ^{40}Ar – ^{39}Ar dating of the epidote–glaucophane, epidote–
130 chlorite and epidote–actinolite schists revealed the cooling ages of 83.5 ± 1.2 Ma, 158.4 ± 4.2
131 Ma, and 187.4 ± 3.7 Ma, respectively whereas phyllite, actinolite schist and amphibole–
132 epidote schist yielded 119.8 ± 3.3 Ma, 177.4 ± 5.8 Ma, 256.9 ± 8.0 Ma, respectively (Tables 2
133 and 3).

134 Overlying the Ankara Mélange tectonically or unconformably are volcanic and volcanoclastic
135 rocks of an island arc origin (Figs. 9 and 10). Nearly 20 km north of Kalecik subalkaline to
136 alkaline volcanic rocks (Dönmez et al., 2009), intercalated with clayey and sandy limestone,
137 calcareous sandstone, pebblestone, sandstone and shale, overlie the Ankara Mélange units
138 and the flyschoidal sedimentary rocks (Hakyemez et al., 1986; Rojay and Süzen, 1997). The
139 volcanic rocks are locally overlain by the Upper Cretaceous reefal limestones and
140 sandstones containing rudist fossils (Fig. 10a and b). Both pillowed and massive lava flows

141 with cooling joints occur (Figs. 9c and 10d); the massive lava flows contain cm-size augite
142 and leucite phenocrysts. Mafic dikes locally crosscut the volcanoclastic rocks of the arc
143 sequence (Fig. 9d). The ^{40}Ar – ^{39}Ar whole-rock dating of an arc-related pillow lava has yielded
144 an age of 67.8 ± 4.9 Ma (Table 4a).

145 Lamprophyre dikes and a syeno-diorite pluton of an island arc origin are intruded into the
146 ophiolitic and seamount rocks and the mélangé matrix along the Kizilirmak River near and
147 east of Kalecik (Fig. 11). The brownish grey colored lamprophyric dikes continue along-strike
148 for 200 to 1000 m, and are displaced by local thrust faults. The ^{40}Ar – ^{39}Ar whole-rock dating
149 and the ^{40}Ar – ^{39}Ar biotite age from the lamprophyric dikes revealed ages of 67.2 ± 1.2 Ma and
150 63.6 ± 1.2 Ma, respectively (Table 4b and c).

151 We have also obtained an ^{40}Ar – ^{39}Ar biotite age of 75.9 ± 1.3 Ma from a syeno-dioritic pluton,
152 approximately 1 km in diameter, indicating that the arc magmatism started as early as the
153 Campanian and that it progressed with alkaline volcanism and dike emplacement throughout
154 the Maastrichtian and Early Paleocene (Table 4d). Andesitic lavas and volcanoclastic and
155 pyroclastic rocks are intercalated with the Upper Cretaceous–lower Paleocene turbiditic
156 rocks in the region. These turbiditic and flyschoidal rocks contain volcanic pebbles in the
157 lower stratigraphic levels and grade upwards into sandstone and shale. The Paleocene rocks
158 (Dizilitaslar Formation) are conformably overlain by the lower to Middle Eocene sandstone,
159 shale, clayey limestone and marl units that collectively make up the Mahmutlar Formation
160 (Akyürek et al., 1984). All these Paleogene sedimentary rocks were deformed by south-
161 vergent thrust faults and folds, indicating that they underwent N–S-directed contractional
162 deformation in the Middle to Late Eocene.

163 **4. Petrography**

164 In this section we describe the primary and secondary mineral assemblages and the textures
165 of the main lithological types associated with the Neotethyan oceanic crust, seamount
166 volcanic units, and island arc assemblages (e.g. volcanic rocks, lamprophyre dikes and
167 syeno-diorite plutons) that we investigated in the study area.

168 **4.1. Basalt**

169 The seamount-related alkaline basaltic rocks consist mainly of plagioclase (55–60%) and
170 clinopyroxene (approximately 40%), displaying an intergranular texture (Fig. 12a). Some of
171 the basalt samples contain olivine phenocrysts (about 15%) ranging in size from 0.2 mm to 2
172 mm. Clinopyroxene grains (titanaugites) are partially altered into chlorite, olivine to

173 serpentine and iddingsite, and plagioclase to sericite and chlorite. Apatite and opaque
174 minerals (Fe–Ti oxide) occur as accessory minerals. Amygdals are filled with secondary
175 carbonate and chlorite minerals.

176 Tholeiitic basaltic rocks of the Neotethyan oceanic crust comprise microlitic plagioclase and
177 clinopyroxene crystals in a fine–grained texture (Fig. 12b). They are partially or completely
178 spilitized, with plagioclase replaced by albite, sericite, chlorite and epidote (saussuritization),
179 whereas clinopyroxene replaced by actinolite (uralitization) and chlorite. The glassy material
180 in the matrix is transformed into chlorite. Leucoxene and opaque minerals are present as
181 accessories. Vesicles in the basaltic lavas are filled by secondary carbonate and chlorite.

182 The island-arc basaltic rocks consist mainly of plagioclase (about 55%) and clinopyroxene
183 (45%) crystals in the porphyritic textures with chloritized glassy and microcrystalline
184 groundmass. Clinopyroxene (diopside) grains range in size from 0.2 mm to 2 mm in length
185 (Fig. 12c and d), and locally display twinning. The plagioclases are partly altered to chlorite
186 and carbonate minerals. Accessory minerals are made of fine crystalline Fe–Ti oxides.
187 Basaltic andesites contain plagioclase, clinopyroxene, minor olivine and biotite within
188 porphyritic and glomeroporphyritic textures (Fig. 12e). Ferromagnesian minerals are locally
189 1.5 cm-long. Fe–Ti oxide minerals are accessories. The groundmass consists of plagioclase
190 microlites, and chloritized and/or devitrified glass. Basaltic lavas include vesicles filled by
191 secondary carbonate, chlorite, and zeolite.

192 **4.2. Basanite**

193 The ultrabasic volcanic rocks consist of clinopyroxene, plagioclase and minor olivine
194 occurring as euhedral and subhedral grains in a hyalomicroclitic, porphyritic texture.
195 Plagioclase forms microlites or micro–phenocrysts, and is commonly altered to clay minerals.
196 Clinopyroxene is mainly augite, and displays zoning and twinning. Olivine is surrounded by a
197 groundmass that is made entirely of serpentine minerals. Small analcime crystals occur as a
198 replacement of leucite between plagioclase and clinopyroxene crystals within the
199 groundmass.

200 **4.3. Tephrite**

201 This fine–grained basaltic rock comprises clinopyroxene (augite), leucite, rare olivine and
202 black mica (phlogopite) crystals within a hyalomicroclitic or porphyritic texture. Plagioclase
203 microlites, ultra fine–grained clinopyroxene, phlogopite, leucite and glassy material form the
204 groundmass, whereas clinopyroxene and leucite occur as euhedral to subhedral

205 microphenocrysts. The leucite contents in the leucite-tephrite rock are up to ~25% (Fig. 12d).
206 Small, anhedral or subhedral opaque minerals are found as accessory minerals.

207 Some tephrites display characteristic features of phonolitic tephrite with feldspar crystals
208 (plagioclase > K-feldspar) and mafic minerals (phlogopite, hornblende) in a microcrystalline
209 porphyritic texture. Plagioclase is partially altered to sericite and chlorite, whereas sanidine is
210 partially altered to sericite and clay minerals. Leucite occurs as subhedral grains, is mostly
211 altered to sanidine microlites, zeolite and clay minerals, and is surrounded by small
212 phlogopite flakes. Euhedral apatite crystals and anhedral opaque minerals (Fe–Ti oxides) are
213 present as accessories.

214 **4.4. Lamprophyre**

215 These alkaline dike rocks consist mainly of small prismatic clinopyroxene (diopside), minor
216 phlogopite and leucite pseudomorphs embedded in a groundmass composed of feldspars
217 (orthoclase>plagioclase), analcime crystals and glassy material (Fig. 12f and g). Both
218 plagioclase and orthoclase are partly or completely altered to carbonate, clay and zeolite
219 minerals; phlogopite is replaced by chlorite along its rims. Small, interstitial apatite laths are
220 enclosed in the orthoclase crystals. In addition, euhedral prismatic apatite crystals up to 0.7
221 mm in length are also present in the groundmass. Opaque minerals occur as accessory
222 crystals.

223 **4.5. Syeno–diorite**

224 The main minerals in this intrusive rock include feldspar (plagioclase ≥ orthoclase),
225 clinopyroxene, hornblende and biotite (Fig. 12h). Subhedral to anhedral plagioclase crystals
226 form a granular texture; some large orthoclase crystals (~2.5 cm) locally give the rock a
227 porphyry texture. Plagioclase grains (An₂₈–An₄₈) are locally surrounded by orthoclase. K–
228 feldspar grains display a perthitic texture. Subhedral to anhedral clinopyroxene (diopside),
229 hornblende and biotite crystals show partial chloritization. Subhedral hornblende crystals
230 have opacite rims around them as a result of metasomatism during their reaction with melt
231 (Plechov et al., 2008). The subhedral prismatic apatite and anhedral granular opaque
232 minerals are present as accessories.

233 **5. Analytical Methods**

234 We analyzed fifty–one (51) rock samples for major, trace, and rare–earth element chemistry
235 at ACME Analytic Laboratory (Canada). Inductively coupled plasma–emission spectroscopy

236 has been used for major–element analysis, and inductively coupled plasma–mass
237 spectroscopy has been used for the analysis of both trace elements and rare–earth elements
238 (REE). The results of these analyses are presented in Tables 5, 6, 7, 8 and 9.

239 $^{40}\text{Ar}/^{39}\text{Ar}$ age dating was done at the Geochronology and Isotopic Geochemistry Laboratory
240 of Activation Laboratories Ltd. (Actlabs), Ancaster, Ontario, Canada. We obtained $^{40}\text{Ar}/^{39}\text{Ar}$
241 ages of biotite separates from two samples of the arc rocks. In addition, whole rock fractions
242 of five rock samples were analyzed. The samples wrapped in Al foil was loaded in evacuated
243 and sealed quartz vial with K and Ca salts and packets of LP–6 biotite interspersed with the
244 samples to be used as a flux monitor. The sample was irradiated in the nuclear reactor for 48
245 hours. The flux monitors were placed between every two samples, thereby allowing precise
246 determination of the flux gradients within the tube. After the flux monitors were run, J values
247 were then calculated for each sample, using the measured flux gradient. LP–6 biotite has an
248 assumed age of 128.1 Ma. The neutron gradient deed not exceeded 0.5% on sample size.
249 The Ar isotope composition was measured in a Micromass 5400 static mass spectrometer.
250 1200°C blank of ^{40}Ar deed not exceed $n \cdot 10^{-10}$ cc STP.

251 Argon is extracted from the sample as degassing at $\sim 100^\circ\text{C}$ during two days in double
252 vacuum furnace at 1700°C . Argon concentration is determined using isotope dilution with
253 ^{38}Ar spike, which is introduced to the sample system prior to each extraction. The obtained
254 pure Ar is introduced into customer build magnetic sector mass spectrometer (Reinolds type)
255 with Varian CH5 magnet. Measurement Ar isotope ratios is corrected for mass–
256 discrimination and atmospheric argon assuming that ^{36}Ar is only from the air. After each
257 analysis the extraction temperature is elevated to 1800°C for few minutes. Then, Aliquot of
258 the sample is weighted into graphite crucible with lithium metaborate/tetraborate flux and
259 fused using LECO induction furnace for K–analysis. The fusion bead is dissolved with acid.
260 Standards, blanks and sample are analyzed on Thermo Jarrell Ash Enviro II ICP
261 Spectrometer.

262 The Sr, Nd, and Pb isotopic compositions of six samples from the alkaline lamprophyric dikes
263 have been determined at the ACT Analytical Laboratories Ltd., Canada (Table 9). The Sr
264 isotope analysis was performed with a Triton multi–collector mass–spectrometer in static
265 mode. The weighted average of 15 SRM–987 Sr–standard runs yielded 0.710258 ± 9 (2s) for
266 $^{87}\text{Sr}/^{86}\text{Sr}$. Sm and Nd were separated by extraction chromatography on hexyl di–ethyl
267 hydrogen phosphate–covered Teflon powder. The analysis was performed on a Triton multi–
268 collector mass spectrometer in static mode. $^{143}\text{Nd}/^{144}\text{Nd}$ ratios are relative to the value of
269 0.511860 for the La Jolla standard. Pb was separated using the ion–exchange technique with

270 Bio–Rad 1x8. Pb isotope compositions were analyzed on Finnigan MAT–261 multicollector
271 mass spectrometer. The measured Pb isotope ratios were corrected for mass fractionation
272 calculated from replicate measurements of Pb isotope composition in the National Bureau of
273 Standards SRM – 982 standards. External reproducibility of lead isotope ratios – $^{206}\text{Pb}/^{204}\text{Pb}$
274 $=0.1\%$, $^{207}\text{Pb}/^{204}\text{Pb}=0.1\%$, $^{208}\text{Pb}/^{204}\text{Pb}=0.2\%$ – on the 2σ level has been demonstrated
275 through multiple analyses of standard BCR–1.

276 **6. Geochemistry**

277 We report below on the geochemistry of the representative samples of oceanic basaltic rocks
278 in the Ankara Mélange, as well as the lamprophyric dikes, a syeno–dioritic pluton, and
279 alkaline lavas that crosscut and/or cover the blocks of volcanic and volcanoclastic rocks,
280 serpentinite, radiolarian chert, and shale in the Ankara Mélange.

281 **6.1. Oceanic Basaltic Rocks**

282 The $\text{Na}_2\text{O}+\text{K}_2\text{O}$ values of basaltic blocks of the Neotethyan oceanic crust range from 1 wt%
283 to 4.28 wt%, with the K_2O values much lower than those of Na_2O (Table 5). The Na
284 enhancement of two samples (CE.07, CE.08) may be a result of spilitization caused by low–
285 grade hydrothermal ocean floor metamorphism. Similarly, the total alkali values from the
286 seamount volcanic blocks vary between 4.72 and 8.14 wt%, with the Na_2O values (3.78–6.79
287 wt%) much higher than that of oceanic crust (Table 6).

288 On the total alkali vs. silica (TAS) diagram the tholeiitic–calcalkaline volcanic and isolated
289 dike rocks from the Tethyan oceanic crust fall in the field of basalt and basaltic andesite,
290 whereas the samples of seamount alkaline rocks plot in the basanite, tephrite ($\text{SiO}_2 = 39.77\text{--}$
291 46.36 wt%), trachyte ($\text{SiO}_2 = 68.47$ wt%), trachybasalt ($\text{SiO}_2 = 50.15$ wt%) and foidite ($\text{SiO}_2 =$
292 39.77 wt%) fields (Fig. 13a and b). The oceanic basalt samples have lower TiO_2 values
293 (0.26–1.74 wt%) in comparison to the alkaline, seamount volcanic rocks (1.64–2.46 wt%),
294 except for a volcanic sample with tholeiitic OIB (Ocean–Island basalt) characteristics. On a
295 Ti–Zr–Y discrimination diagram (Pearce and Cann, 1973), the oceanic basalt samples plot in
296 the MORB (mid–ocean ridge basalt) and island arc tholeiite (IAT) fields, whereas the
297 seamount volcanic rocks generally fall in the within–plate alkali basalt field (except a trachyte
298 sample; Fig. 13c). On a Ti–V diagram (Shervais, 1982), the samples of oceanic basaltic
299 rocks mostly plot in the MORB field ($\text{Ti}/\text{V} = 22.6\text{--}28.9$), whereas four samples have island arc
300 tholeiite to boninitic affinities ($\text{Ti}/\text{V} = 5.4\text{--}25.55$) (Fig. 13d). The samples of silica–
301 undersaturated, seamount volcanic rocks display an OIB–character with high Ti/V ratios
302 (62.6–261.2).

303 The N–MORB normalized multi–element diagrams of the representative samples of basalts
304 of oceanic crust and seamount volcanic rocks are shown in Fig. 13e. Basaltic samples of
305 both MORB and SSZ (suprasubduction zone) affinities show enrichment in their LILE (the
306 large ion lithophile elements: Rb, Ba, K, Sr, Cs, Th) contents. The HFSE (high field strength
307 elements: Nb, Ta, Zr, Hf, Ti, Y) and REE (rare earth elements) contents of the MORB–type
308 basaltic rocks display a slight increase, whereas the SSZ–related basaltic rocks (four
309 samples) exhibit depletion in HFSE and REE. The LILE, HFSE, LREE (light–REE) contents
310 of the seamount volcanic rocks are extremely enriched relative to the HREE (heavy–REE)
311 values. Also, the Th/Yb (2.8–5.6) and Nb/Yb (27.6–54.8) values of the seamount volcanic
312 rocks are high in comparison to those of the Neotethyan oceanic basalt samples
313 (Th/Yb=0.2–1.1; Nb/Yb=0.7–2.7). However, the alkaline lava samples have the ratios of
314 Nb/Y>1.5 and Zr/Nb<6 that are typical for within–plate basalts (Edwards et al., 1991). The
315 seamount volcanic rocks have Nb/Y ratios of 2.3–3.1 and Zr/Nb ratios of 3.1–4.1, indicating
316 OIB–like geochemical characteristics, whereas the oceanic basalt samples have Nb/Y (0.1–
317 0.4) and Zr/Nb (8.1–32) values characteristic of island–arc rocks.

318 **6.2. Island Arc Rocks**

319 A small syeno–diorite pluton, a suite of volcanic rocks, and lamprophyric dikes in the Kalecik
320 (Ankara) area collectively represent the products of island arc magmatism. These arc rocks
321 mostly plot in the alkaline field on a TAS diagram (Fig. 14a and b). The alkaline rock samples
322 with medium to high Al₂O₃ contents (10–19 wt%) represent both silica–saturated and silica–
323 undersaturated rock units (Tables, 7, 8 and 9). The lamprophyric dikes have picobasalt,
324 trachybasalt, trachyandesite, tephrite and phonotephrite compositions, whereas the volcanic
325 rocks display basalt, basanite, tephrite, leucite tephrite and foidite compositions. The
326 samples from small alkaline intrusions fall into the syeno–diorite field in the TAS diagram
327 (Fig. 14b; Cox et al., 1979). The Late Cretaceous–Early Paleocene volcanic rocks (andesite,
328 dacite, rhyolite), found nearly 60 km SW of Kalecik, show subalkaline (tholeiitic and calc–
329 alkaline) compositions, except for a few trachytbasalt and trachyandesite samples (Fig. 14a,
330 c and d; Dönmez et al., 2009).

331 The alkaline volcanic rocks mostly display high–K shoshonitic compositions in the K₂O vs.
332 SiO₂ diagram (Fig. 14d; Peccerillo and Taylor, 1976). Some volcanic and dike rocks also plot
333 in the fields of medium– high–K, calc–alkaline series. Although some alkaline volcanic rocks
334 show medium–K calc–alkaline characteristics as a result of hydrothermal alteration (LOI/loss
335 on ignition>2wt%), they have high–K shoshonitic affinity since the leucite bearing, silica–
336 undersaturated alkaline rocks experienced analcimization resulting in low K₂O values in favor

337 of Na₂O values. On the Hastie et al. (2007), and Pearce (1982) diagrams, which utilize the
338 immobile elements and the ratios of immobile elements (Th vs. Co, and Ce/Yb vs. Ta/Yb),
339 the arc-related plutonic, volcanic and dike rocks generally display high-K (K₂O/Na₂O = 1.5–
340 3.4) and shoshonitic characteristics (Fig. 14e and f). However, seven samples from the
341 volcanic rocks and lamprophyre dikes contain high K₂O/Na₂O ratios (18.16–24.52) showing
342 ultrapotassic (K₂O/Na₂O>3) characteristics.

343 When plotted on MgO vs. major element diagrams, the analyzed samples mainly exhibit
344 negative correlations, except on the Fe₂O₃ and TiO₂ plots, which show positive correlations
345 (Fig. 15). Based on the MgO vs. trace element variation diagrams (Fig. 15), Co shows a
346 positive trend while Ba, Rb, Sr, Th and Zr all exhibit negative trends. These major and trace
347 element trends can be explained by fractionation of clinopyroxene, feldspar, black mica
348 (biotite, phlogopite), Fe–Ti oxides and apatite. However, the scatter in Fig. 15 may also be
349 caused by the alteration of the arc rocks and/or the involvement of subducted sediments in
350 their melt regime. The rock samples from the small syeno–diorite pluton with metaluminous
351 characteristics plot in the VAG (volcanic arc granites) field (Fig. 16a, b and c). The Ti–Zr–Y
352 and Ti–V diagrams (Pearce and Cann, 1973; Shervais, 1982) show that the alkaline basic
353 samples and the subalkaline volcanic rocks (Dönmez et al., 2009) from the southwestern
354 part of the study area all plot in the arc field (Fig. 16d and e), whereas the TiO₂–Al₂O₃ and Y–
355 Zr diagrams (Muller et al., 1992) show that these samples fall into the arc field (Fig. 16f and
356 g). The analyzed alkaline rocks display shoshonitic characteristics in the Th/Yb vs. Nb/Yb
357 diagram (Pearce, 2008), and their Hf/Th ratios are rather low ranging from 0.11 to 0.57,
358 consistent with their shoshonitic affinity. The island–arc tholeiitic (IAT) basaltic rocks have
359 Hf/Th>3, whereas the calc–alkaline volcanic rocks have Hf/Th<3 (Wood, 1980). Their Th
360 enrichment and increased Th/Yb ratios along the mantle metasomatism trend indicate the
361 influence of subduction–derived fluids in their magma source (Fig. 16h; Pearce, 2008). The
362 samples derived from the blocks of N–MORB–, SSZ– and OIB–like oceanic basalts in the
363 Ankara Mélange typically plot within the MORB–OIB mantle array (Fig. 16h).

364 The primitive mantle–normalized, multi–element diagrams of the representative samples
365 from the high–K shoshonitic arc rocks around Kalecik (Ankara), Yapraklı (Çankırı) and
366 Laloğlu (Çorum) are plotted in Fig. 17a. The trace element patterns of all the analyzed
367 alkaline rocks display strong enrichment of the LILE, LREE and also Pb, U in comparison to
368 HFSE (Nb, Ta, Zr, Hf, Ti, Y), which show negative anomalies indicating subduction zone
369 influence (Kempton et al., 1991). The high Ba/Ta (>450) and Ba/Nb (>28) ratios are
370 characteristic features of subduction–related magmas (Fitton et al., 1988). The very high
371 ratios of Ba/Ta (383–5255), Ba/Nb (64–538), and relatively high Zr/Nb (5–22), Th/Yb (2–14),

372 Zr/Y (3–7) and La/Yb (9–36) have been attributed to a mantle source, which was enriched by
373 a subduction component (Frey et al., 1978; Fitton et al., 1988; Maury et al., 1992; Schiano et
374 al., 1995). However, some of the lamprophyre dike samples (DM.2, DM.6, DM.8, DM.9,
375 DM.10) contain La/Yb ratios of 30, indicating highly undersaturated magmas for their origin.
376 Also, the alkaline rocks with Mg # <61, except for one sample (Mg# = 71), [MgO/(MgO × 0.8
377 $\hat{\text{FeO}}$ total)], imply that none of these shoshonitic rocks represents primary mantle-derived
378 subduction-related magmas. However, their chondrite-normalized REE patterns (Fig. 17b)
379 show LREE enrichment, flat HREE (La/Sm_n=2.18–5.71; Gd/Lu_n=1.69–4.14; La/Lu_n=6.57–
380 24.72), and minor negative Eu anomalies (Eu/Eu*=0.77–0.95). These geochemical
381 characteristics are compatible with those defining subduction-related, arc volcanic
382 assemblages (Tatsumi et al., 1986; Kelemen et al., 1993; Hawkesworth et al., 1993; Pearce
383 and Peate, 1995).

384 The high-K shoshonitic lamprophyric dikes are characterized by intermediate ¹⁴³Nd/¹⁴⁴Nd
385 (0.512674–0.512690) and ⁸⁷Sr/⁸⁶Sr (0.704697–0.704892) isotopic compositions. The initial
386 ε_{Nd} values range from +1.3 to +1.7, whereas the modern ε_{Nd} values vary between +0.7 and
387 +1.0 indicating a relatively enriched mantle source. Their Pb isotope ratios range from 19.332
388 to 19.939 for ²⁰⁶Pb/²⁰⁴Pb, 15.655 to 15.691 for ²⁰⁷Pb/²⁰⁴Pb, and 39.192 to 39.612 for
389 ²⁰⁸Pb/²⁰⁴Pb. The high ²⁰⁶Pb/²⁰⁴Pb, and relatively high ¹⁴³Nd/¹⁴⁴Nd and ⁸⁷Sr/⁸⁶Sr ratios seem to
390 be compatible with a mantle source that is enriched by slab-derived fluids and/or subducted
391 pelagic sediments.

392 **7. Discussion**

393 **7.1. Source Characteristics**

394 The subduction-accretion complex represented by the Ankara Mélange contains blocks of
395 oceanic lithosphere showing geochemical affinities ranging from MORB to IAT and calc-
396 alkaline. The SSZ-type ophiolite assemblages in the melange display both IAT-like and
397 boninitic geochemical signatures. The ophiolitic units with an IAT-like chemistry are the
398 manifestation of partial melting of the upper mantle peridotites, which were modified by
399 incompatible element-enriched hydrous fluids (or melt) released from the subducting
400 Tethyan oceanic slab. The ophiolitic units with MORB-like signatures represent the products
401 of a depleted mantle source. Some of the samples with MORB-like chemistry plot within or
402 near the IAT field (Figs.13c and 16h) indicating that their magmas were influenced by
403 subduction-derived fluids. These ophiolitic rocks are the oldest units as constrained by the
404 volcanic stratigraphy and crosscutting relationships. Some doleritic dikes and basaltic rocks

405 in the ophiolites show boninitic affinities, consistent with their formation in a forearc setting
406 (Dilek and Furnes, 2011; Sarifakioglu et al., 2011). Collectively, the ophiolitic units in the
407 Ankara mélangé display a geochemical progression that is typical of the development of
408 forearc oceanic crust in the early stages of subduction-induced magmatism, as also
409 documented from other Tethyan ophiolites (Dilek and Furnes, 2009, 2011; Dilek and Thy,
410 2009; Pearce and Robinson, 2010; Saccani et al., 2011; Moghadam et al., 2013).

411 Seamount volcanic rocks occurring in the Ankara mélangé have OIB-like geochemical
412 features, showing tholeiitic to alkaline affinities (Fig. 13e) with enrichment in incompatible
413 elements and LREEs. The tholeiitic OIB affinity of some of the seamount volcanic rocks may
414 have resulted from the interaction of plume-derived melts with MORB-type melts near a
415 seafloor spreading system. The depletion of the OIB-type volcanic rocks in immobile
416 elements (especially Ti) suggests mixing of the plume and MORB-type melts during
417 seamount evolution.

418 The high-K alkaline rocks exhibit LILE and HFSE enrichments and negative Nb, Ta, Hf, Zr,
419 Ti anomalies, indicating strong subduction influence in their melt evolution (Fig. 17a). The
420 high ratios of LILE/HFSE ($Ba/Nb = 64\text{--}538$; $Ba/Ta = 383\text{--}5255$; $Rb/Nb = \sim 2\text{--}20$),
421 LREE/HFSE ($La/Nb = 1.8\text{--}7.2$; $La/Ta = 48\text{--}188$; $La/Sm_n \sim 4$), LILE/LREE ($Th/La = 0.16\text{--}0.49$)
422 and $Zr/Nb (5\text{--}22)$, and the large negative Nb-Ta anomaly in the multi-element diagrams all
423 point to a melt source affected by subduction-generated fluids and/or crustally contaminated
424 magmas. The observed high $Ba/Nb (64\text{--}538)$, $La/Yb (9\text{--}36)$, $Sr/Nd (14\text{--}45)$ and $Ce/Yb (20\text{--}$
425 $73)$ ratios, and low $Nb/U (2\text{--}7)$, $Ba/La (20.02\text{--}59.83)$, $U/Th (0.13\text{--}0.50)$ and $Ce/Pb (\sim 2\text{--}20)$
426 values indicate that the mantle melt source may have been modified by some melts derived
427 from relatively incompatible element-rich, subducted pelagic and/or terrigenous sediments.
428 In contrast, the high $Ce/Pb (25+5)$ and $Nb/U (47+10)$ ratios observed in the OIB-type
429 seamount volcanic rocks indicate that the magmas of these rocks were not modified by
430 subducted sediments (Hoffman et al., 1986).

431 Enrichments in Cs, Rb, Ba, Th, U, K, La, Ce and Pb of the alkaline rocks suggest that their
432 melt source was modified by subducted slab material (mainly fluids, and pelagic and/or
433 terrigenous sediments). Slab-derived fluids helped to form hydrous and K-rich minerals,
434 such as amphibole, apatite and phlogopite with high $Rb/Sr (0.04\text{--}0.71)$ and $K/Ti (3.77\text{--}16.62)$
435 ratios relative to MORB- and OIB-like magmas, and resulted in a positive correlation
436 between Ba/Nb and La/Nb ratios (Fig. 18a). Also, the high $La (18.4\text{--}69.2 \text{ ppm})$ contents and
437 La/Yb ratios ($9.5\text{--}34.6$) reflect that the high-K magmas may have been produced by small
438 degrees of partial melting of a subduction-metasomatised mantle source (Fig. 18b).

439 As illustrated in the $^{143}\text{Nd}/^{144}\text{Nd}$ vs. $^{87}\text{Sr}/^{86}\text{Sr}$ diagram (Fig. 19a), six lamprophyre samples plot
440 on the mantle array defining a subduction component during the evolution of their magmas.
441 We also show in this diagram, for comparison, the Late Cretaceous–Early Tertiary volcanic
442 rocks from the southern part of Central Anatolia and the Eastern Pontides, and the Cenozoic
443 volcanic units in Western Anatolia (Alpaslan et al., 2004; 2006; Eyüboğlu, 2010; Altunkaynak
444 and Dilek, 2006 and references therein). The relatively high Pb (up to 34 ppm in some
445 samples) and $^{87}\text{Sr}/^{86}\text{Sr}$ contents, and the Rb/Sr ratios (0.02–0.71) of the lamprophyre rocks
446 also indicate the effects of subducted oceanic sediments added to the mantle melt source
447 (Pearce and Peate, 1995). In the $^{206}\text{Pb}/^{204}\text{Pb}$ vs. $^{208}\text{Pb}/^{204}\text{Pb}$, $^{206}\text{Pb}/^{204}\text{Pb}$ vs. $^{207}\text{Pb}/^{204}\text{Pb}$,
448 $^{87}\text{Sr}/^{86}\text{Sr}$ vs. $^{206}\text{Pb}/^{204}\text{Pb}$ and $^{143}\text{Nd}/^{144}\text{Nd}$ vs. $^{206}\text{Pb}/^{204}\text{Pb}$ variation diagrams, the data points lie
449 above the Northern Hemisphere Reference Line (NHRL), and the radiogenic isotope data fall
450 close to the fields of MORB, enriched lithospheric mantle source (EMII) and oceanic
451 sediments. These features collectively suggest that the magmas of the lamprophyre rocks
452 were derived from a MORB–like mantle source that was enriched by subducted terrigenous
453 and carbonate sediments (Fig. 19b–e). However, the post–collisional Late Cretaceous–Early
454 Tertiary volcanic rocks in the Ulukisla basin in the southern part of Central Anatolia have
455 higher $^{87}\text{Sr}/^{86}\text{Sr}$ and lower $^{143}\text{Nd}/^{144}\text{Nd}$ ratios than those of the lamprophyres in the Ankara
456 Mélange, indicating an EMII with recycled, continent–derived material. The late Cretaceous
457 high–K volcanic rocks representing active continental margin arc units in the Eastern
458 Pontides with low $^{87}\text{Sr}/^{86}\text{Sr}$ reflect a mantle source enriched by continental crustal rocks. The
459 $^{143}\text{Nd}/^{144}\text{Nd}$, $^{87}\text{Sr}/^{86}\text{Sr}$, $^{206}\text{Pb}/^{204}\text{Pb}$, $^{208}\text{Pb}/^{204}\text{Pb}$ and $^{207}\text{Pb}/^{204}\text{Pb}$ values reflecting subduction
460 enrichment and crustal contamination of the source of the post–collisional, Middle Eocene
461 volcanic units in Central Anatolia and the Tertiary volcanic suites in western Anatolia have
462 been explained by slab breakoff–induced asthenospheric upwelling and associated partial
463 melting of the orogenic lithospheric mantle (Alpaslan et al., 2004, 2006; Altunkaynak and
464 Dilek, 2006, 2013; Dilek and Altunkaynak, 2007; Keskin et al., 2008; Gündoğdu–Atakay,
465 2009; Sarifakioglu et al., 2013).

466 The depletion of HFSE with respect to LREE enrichment, and high LILE/HFSE and
467 radiogenic isotope ratios suggest that the high–K shoshonitic rocks are likely to have formed
468 by small degrees of partial melting of a lithospheric mantle modified by slab–derived hydrous
469 fluids.

470

471 **7.2. Tectonic Model**

472 The Ankara Mélange displays a heterogeneous structural architecture containing oceanic
473 and crustal rocks with different internal structure, stratigraphy and geochemical
474 compositions. The oldest ophiolitic rocks in the Ankara Mélange appear to have formed in a
475 SSZ setting within the Northern Tethys around 180 Ma (Dilek and Thy, 2006; Sarifakioglu et
476 al., 2011). The ~80 Ma (80.3 ± 7.6 Ma) ophiolitic rocks in the same mélange also indicate that
477 oceanic crust formation in the Northern Tethys was still in operation in the Late Cretaceous
478 (Table 1).

479 We obtained Middle–Upper Triassic biostratigraphic age data from the neritic limestones that
480 are spatially associated with the seamount volcanic rocks, indicating that an oceanic
481 lithosphere of the Late Triassic and older ages must have existed in this ocean to make up
482 the substratum of the seamounts. Thus, we know that the northern branch of Neotethys was
483 already a wide–open ocean with its MORB–type oceanic lithosphere between the Pontide
484 block to the north and the Anatolide–Tauride micro–continent to the south in the Early
485 Triassic (or even before). The ophiolitic mélange units in the Kırıkkale–Ankara–Çankırı–
486 Çorum area are unconformably overlain by basal volcanic conglomerates of an arc origin.
487 The overlying volcanosedimentary units contain clayey– and sandy–limestone, limey
488 sandstone, and sandstone–claystone alternating with volcanoclastic rocks. These rock types
489 and their internal stratigraphy suggest their deposition in a frontal arc–forearc basin. The
490 clayey limestones are intruded by dikes and sills and have Late Santonian, and Campanian–
491 Maastrichtian ages based on their fossil contents (Sarifakioglu, unpublished data). The
492 radiometric age data from an alkaline basaltic rock (YK.4) and a syeno–diorite intrusion
493 (YK.438) give ages of 67.8 ± 4.9 Ma and 75.9 ± 1.3 Ma, respectively (Table 4a and d),
494 constraining the timing of intra–oceanic arc magmatism as the Latest Cretaceous.

495 In general, subalkaline (tholeiitic and calcalkaline) volcanic arc rocks occur in the northern
496 part of the study area, whereas the younger alkaline volcanic and plutonic rocks in the south.
497 We interpret this spatial and temporal relationship to have resulted from a southward
498 progression of the arc magmatism from subalkaline to alkaline affinities through time due to
499 arc rifting above the southward retreating Tethyan subduction system (Fig. 20). We,
500 therefore, think that the arc–related late alkaline dikes and plutons were emplaced on and
501 across the evolving subduction–accretion complex above the north–dipping, southward
502 rolling Tethyan slab.

503 The high-K and shoshonitic Eocene dikes and lavas in the Ankara mélange formed from
504 melts derived from partial melting of the metasomatized arc mantle that was triggered by the
505 influx of slab breakoff-induced asthenospheric flow. This slab breakoff was a result of an arc-
506 continent (Central Anatolian Crystalline Complex – CACC) collision, followed by the
507 continent–continent collision (Sakarya and CACC) in the Early to Middle Eocene.

508 **8. Conclusions**

509 1. Blocks of Middle–Late Triassic seamount and Upper Permian metamorphic rocks
510 occurring in the Ankara Mélange represent an intra–oceanic subduction–accretion
511 complex that developed in the Northern Tethys during the late Paleozoic through
512 Cretaceous.

513 2. Thrust sheets and/or megablocks containing SSZ ophiolite units with Liassic and
514 Cretaceous ages were incorporated into this subduction–accretion complex during the
515 early Late Cretaceous.

516 3. The Late Cretaceous tholeiitic to calc–alkaline volcanic rocks are the products of an
517 intra–oceanic island arc system. The tholeiitic and calc-alkaline arc rocks show
518 enrichment in incompatible elements due to the influence of slab-derived fluids. The
519 shoshonitic arc rocks representing the latest stage of island arc magmatism were
520 produced by partial melting of a subduction–enriched mantle source.

521 **Acknowledgements**

522 This study was supported by a grant from the General Directorate of Mineral Research and
523 Exploration of Turkey (MTA, Ankara; Project no: 2007–2008.30.1601.d–f). We thank Dr.
524 Yakov Kapusta (ACTLabs, Canada) for the radiometric and isotopic analyses of our rock
525 samples in a timely fashion, and for his help with the interpretation of the obtained data. We
526 extend our appreciation to the referee, Dr. Ibrahim Uysal (Blacksea Technical University,
527 Turkey). Special thanks are due to Dr. Francesca Funiciello for her editorial suggestions,
528 which improved the manuscript. We would like to acknowledge the Head of the Geological
529 Research Department, Dr. Erol Timur, in MTA-Ankara for his continued support of our
530 *Ophiolite Inventory Project* in Turkey over the last two years.

531

532 **References**

- 533 Akyürek, B., Bilginer, E., Akbaş, B., Hepşen, N., Pehlivan, Ş., Sunu, O., Soysal, T., Dağer, Z.,
534 Çatal, E., Sözeri, B., Yıldırım, H. and Hakyemez, Y.: Fundamental geological
535 characteristics of Ankara–Elmadağ–Kalecik area. *Journal of Geological Engineering*
536 (*Jeoloji Mühendisliği Dergisi*), Chamber of Geological Engineers of Turkey (TMMOB
537 Jeoloji Mühendisleri Odası), 20, 31–46, 1984 (in Turkish with English abstract).
538
- 539 Alpaslan, M., Boztug, D., Frei, R., Temel, A. And Kurt, M.A.: Geochemical and Pb–Sr–Nd
540 isotopic composition of the ultrapotassic volcanic rocks from the extension–related
541 Çamardı–Ulukisla basin, Nigde Province, Central Anatolia, Turkey. *Journal of Asian*
542 *Earth Sciences* 27, 613–627, 2006.
- 543 Alpaslan, M., Frei, R., Boztug, D., Kurt, M.A. and Temel, A.: Geochemical and Pb–Sr–Nd
544 isotopic constraints indicating an enriched–mantle source for Late Cretaceous to Early
545 Tertiary volcanism, Central Anatolia, Turkey. *International Geology Review* 46, 1023–
546 1041, 2004.
- 547 Altunkaynak, S., and Dilek, Y.: Timing and nature of postcollisional volcanism in Western
548 Anatolia and geodynamic implications, in: *Postcollisional Tectonics and Magmatism in*
549 *the Mediterranean Region and Asia*, edited by: Dilek, Y. and Pavlides, S., Geological
550 Society of America Special Paper 409, 321–351, 2006.
- 551 Altunkaynak, Ş. and Dilek, Y.: Eocene mafic volcanism in northern Anatolia: its causes and
552 mantle sources in the absence of active subduction. *International Geology Review* 55
553 (13), 1641-1659, 2013.
- 554 Bailey, E.B. and McCallien, W.S.: The Ankara Mélange in Central Anatolia. *Bulletine of*
555 *Mineral Research and Exploration Institute, Maden Tetkik ve Arama Enstitüsü, Ankara,*
556 *Turkey*, 40, 12-22, 1950.
- 557 Bailey, E.B. and McCallien, W.S.: The Ankara Mélange and Anatolia Thrust. *Nature* 166,
558 938–941, 1953.
- 559 Bingöl, E., Akyürek, B. and Korkmazer, B.: Geology of Biga Peninsula and characteristics of
560 Karakaya formation. *Geoscience Congress of 50th Anniversary of the Turkish*
561 *Republic, Ankara, 1975, the Publications of MTA General Directorate, 70–77 (in Turkish*
562 *with English abstract), 1975.*

- 563 Boztug, D.: S–I–A type intrusive associations: geodynamic significance of synchronism
564 between metamorphism and magmatism in Central Anatolia, Turkey, in: Tectonics and
565 Magmatism in Turkey and the Surrounding Area, edited by: Bozkurt, E., Winchester, J.
566 A., and Piper, J. D. A., Geological Society of London Special Publication, 173, 441–
567 458, 2000.
- 568 Çoğulu, E., Delaloye, M. and Chessex, R.: Sur l'âge de quelques roches plutoniques acides
569 dans region d'Eskisehir, Turquie, Archives des Sciences, Genève, 18, 692–699, 1965.
- 570 Cox, K.G., Bell, J.D. and Pankhurst, R.J.: The interpretation of igneous rocks. Allen and
571 Unwin, London, 450p, 1979.
- 572 Dangerfield, A., Harris, R. Sarifakioglu, E. and Dilek, Y.: Tectonic evolution of the Ankara
573 Mélange and associated Eldivan ophiolite near Hançili, Central Turkey. Geological
574 Society of America Special Paper 480, 143–169, 2011.
- 575 Delaloye, M. and Bingöl, E.: Granitoids from western and Northwestern Anatolia:
576 Geochemistry and modelling of geodynamic evolution. International Geology Review
577 42, p. 241–268, doi:10.1080/00206810009465081, 2000.
- 578 Dilek, Y. and Altunkaynak, Ş.: Cenozoic Crustal Evolution and Mantle Dynamics of Post–
579 Collisional Magmatism in Western Anatolia. International Geology Review 49, 431–453,
580 2007.
- 581 Dilek, Y. and Thy, P.: Age and petrogenesis of plagiogranite intrusions in the Ankara
582 Mélange, central Turkey. Island Arc 15, 44–57, 2006.
- 583 Dilek, Y. and Furnes, H.: Ophiolite genesis and global tectonics: Geochemical and tectonic
584 fingerprinting of ancient oceanic lithosphere. Geological Society of America Bulletin
585 2011;123;387–411, doi: 10.1130/B30446.1, 2011.
- 586 Dilek, Y. and Furnes, H.: Structure and geochemistry of Tethyan ophiolites and their
587 petrogenesis in subduction rollback systems. Lithos 113, 1–20, 2009.
- 588 Dilek, Y. and Thy, P.: Island arc tholeiite to boninitic melt evolution of the Cretaceous Kizildag
589 (Turkey) ophiolite: Model for multi–stage early arc–forearc magmatism in Tethyan
590 subduction factories. Lithos 113, 68–87, 2009.
- 591 Dönmez, M., Akçay, A.E., Türkecan, A., Evcimen, Ö., Atakay, E. and Görmüş, T.: Tertiary
592 Volcanites in Ankara surroundings. Mineral Research and Exploration Institute of

- 593 Turkey (MTA) Report, No. 11164, 116 pp., Ankara, Turkey, 2009 (in Turkish,
594 unpublished).
- 595 Eyüboğlu, Y.: Late cretaceous high-K volcanism in the eastern pontide orogenic belt:
596 implications for the geodynamic evolution of NE Turkey. *International Geology Review*
597 52(2-3), 142-186, 2010.
- 598 Fitton, J.G., James, D., Kempton, P.D., Ormerod, D.S. and Leeman, W.P.: The role of
599 lithospheric mantle in the generation of Late Cenozoic basic magmas in the Western
600 United States, *J. Petrol., Special Lithosphere Issue*, 331–349, 1988.
- 601 Frey, F.A., Green, D.H. and Roy, S.D.: Integrated models of basalt petrogenesis: A study of
602 Quartz tholeiite to olivine melilites from southeastern Australia utilizing geochemical
603 and experimental data. *Journal of Petrology* 19, 463–513, 1978.
- 604 Güleç, N.: Rb–Sr isotope data from the Agacoren granitoid (East of Tuz Gölü):
605 Geochronological and genetical implications. *Turkish Journal of Earth Sciences* 3, 39–
606 43, 1994.
- 607 Gündoğdu–Atakay, E.: Geological and petrological characteristics of volcanic rocks at
608 southwest of Çorum and geotectonic studies at Alaca höyük excavation site. PhD
609 Thesis, Ankara University, Ankara, Turkey, 194pp., 2009.
- 610 Hakyemez, Y., Barkurt, M.Y., Bilginer, E., Pehlivan, Ş., Can, B., Dağer, Z. and Sözeri, B.:
611 The geology of Yapraklı–Ilgaz–Çankırı–Çandır surroundings. Mineral Research and
612 Exploration Institute of Turkey (MTA) Report, No. 7966, Ankara, Turkey, 1986 (in
613 Turkish, unpublished).
- 614 Hastie, A.R., Kerr, A.C., Pearce, J.A. and Mitchell, S.F.: Classification of Altered Volcanic
615 Island Arc Rocks using Immobile Trace Elements: Development of the Th–Co
616 Discrimination Diagram. *Journal of Petrology* 48 (12), 2341–2357, 2007.
- 617 Hawkesworth, C.J., Gallagher, K., Hergt, J.M. and McDermott, F.: Mantle and slab
618 contributions in arc magmas. *Annual Review of Earth and Planetary Sciences* 21, 175–
619 204, 1993.
- 620 Hoffman, A.W., Jochum, K.P., Seufert, M. and White, W.M.: Nb and Pb in oceanic basalts:
621 New constraints on mantle evolution. *Earth and Planetary Science Letters* 90, 421–436,
622 1986.

- 623 Ilbeyli, N., Pearce, J.A., Thirwall, M.F. and Mitchell, J.G.: Petrogenesis of collision-related
624 plutonics in Central Anatolia, Turkey. *Lithos* 72, 163–182, 2004.
- 625 Irvine, T.N. and Baragar, W.R.A.: A guide to the chemical classification of the common
626 volcanic rocks, *Canadian Journal of Earth Sciences*, 8, 523–548, doi:10.1139/e71-055,
627 1971.
- 628 Kadioglu, Y.K., Dilek, Y., and Foland, K.A.: Slab breakoff and syncollisional origin of the Late
629 Cretaceous magmatism in the Central Anatolian Crystalline Complex, Turkey, in Dilek,
630 Y., and Pavlides, S., eds., *Postcollisional tectonics and magmatism in the
631 Mediterranean Region and Asia*. Geological Society of America, Special Paper 409,
632 381–415, doi:10.1130/2006/2409(19), 2006.
- 633 Kadioglu, Y.K., Dilek, Y., Güleç, N. and Foland, K.A.: Tectonomagmatic evolution of bimodal
634 plutons in the Central Anatolian Crystalline Complex, Turkey. *Journal of Geology* 111,
635 671–690, 2003.
- 636 Kelemen, P.B., Shimizu, N. and Dunn, T.: Relative depletion of niobium in some arc magmas
637 and the continental crust: partitioning of K, Nb, La and Ce during melt/rock reaction in
638 the upper mantle. *Earth and Planetary Science Letters* 120, 111–134, 1993.
- 639 Kempton, P.D., Fitton, J.G., Hawkesworth, C.J. and Ormerod, D.S.: Isotopic and trace
640 element constraints on the composition and evolution of the lithosphere beneath the
641 southern United State. *Journal of Geophysical Research* 96, 13713–13735, 1991.
- 642 Keskin, M., Genç, C.Ş and Tüysüz, O.: Petrology and geochemistry of post-collisional
643 Middle Eocene volcanic units in North–Central Turkey: Evidence for magma generation
644 by slab breakoff following the closure of the Northern Neotethys Ocean. *Lithos* 104,
645 267–305, 2008.
- 646 Koçyiğit, A.: An example of an accretionary forearc basin from northern Central Anatolia and
647 its implications for the history of the Neo–Tethys in Turkey. *Geological Society of
648 America*, Special Paper 103, 22–36, 1991.
- 649 Le Bas, M.J., Le Maitre, R.W., Streckeisen, A. and Zanettin, B.: A chemical classification of
650 volcanic rocks based on total Alkali–Silica content. *Journal of Petrology* 27, 745–750,
651 1986.

- 652 Maury, R.C., Defant, M.J. and Joron, J.L.: Metasomatism of arc mantle inferred from trace
653 elements in Philippine xenoliths. *Nature* 360, 661–663, doi: 10.1038/360661a0, 1992.
- 654 Moghadam, H. S., Stern R.J., Chiaradia, M. and Rahgoshay, M.: Geochemistry and tectonic
655 evolution of the Late Cretaceous Gogher-Baft ophiolite, Central Iran, *Lithos*, 168, 33–
656 47, doi:10.1016/j.lithos.2013.01.013, 2013.
- 657 MTA: The geological map of Turkey, 1/500 000 scaled, Geological Survey of Turkey, The
658 General Directorate of Mineral Research and Exploration, Ankara, Turkey, 2001.
- 659 Muller, D., Rock, N.M.S. and Groves, D.I.: Geochemical discrimination between shoshonitic
660 and potassic volcanic rocks in different tectonic settings: a pilot study. *Mineralogy and
661 Petrology* 46, 259–289, 1992.
- 662 Norman, T.N.: The role of the Ankara Melange in the development of Anatolia (Turkey), in:
663 The Geological Evolution of the Eastern Mediterranean, edited by: Dixon, J. E., and
664 Robertson, A. H. F., Geological Society of London Special Publication, 17, 441–447,
665 1984.
- 666 Nzegge, O. M., Satir, M., Siebel, W., and Taubald, H.: Geochemical and isotopic constraints
667 on the genesis of the Late Palaeozoic Deliktas, and Sivrikaya granites from the
668 Kastamonu granitoid belt (Central Pontides, Turkey). *Neues Jahrbuch Mineralogische
669 Abhandlungen* 183, p. 27–40, 2006.
- 670 Okay, A.I., and Göncüoğlu, M.C.: Karakaya Complex: A review of data and concepts. *Turkish
671 Journal of Earth Sciences* 13, p. 77–95, 2004.
- 672 Okay, A.I., Monod, O. and Monié, P.: Triassic blueschists and eclogites from northwest
673 Turkey: vestiges of the Paleo–Tethyan subduction. *Lithos* 64, 155–178, 2002.
- 674 Okay, A.I., Tüysüz, O., Satir, M., Özkan–Altiner, S., Altiner, D., Sherlock, S. and Eren, R.H.:
675 Cretaceous and Triassic subduction–accretion HP–LT metamorphism and continental
676 growth in the Central Pontides, Turkey. *Geological Society of America Bulletin* 118, p.
677 1247–1269, doi:10.1130/B25938.1, 2006.
- 678 Pearce, J.A.: Trace element characteristics of lavas from destructive plate boundaries. In:
679 Thorpe, R.S. (ed), *Andesites: orogenic andesites and related rocks*. John Wiley &
680 Sons, Chichester, 525–548, 1982.

- 681 Pearce, J.A.: Geochemical fingerprinting of oceanic basalts with applications to ophiolite
682 classification and the search for Archean oceanic crust. *Lithos* 100, 14–48, 2008.
- 683 Pearce, J.A. and Cann, J.R.: Tectonic setting of basic volcanic rocks determined using trace
684 element analyses. *Earth and Planetary Scientific Letters* 19, 290–300, 1973.
- 685 Pearce, J.A. and Peate, D.W.: Tectonic implications of the composition of volcanic arc
686 magmas. *Annual Review of Earth and Planetary Sciences* 23, 251–285, doi:
687 10.1146/annurev.earth.23.050195.001343, 1995.
- 688 Pearce, J. A. and Robinson, P. T.: The Troodos ophiolitic complex probably formed in a
689 subduction initiation, slab edge setting. *Gondwana Research* 18 60–81.
690 10.1016/j.gr.2009.12.003, 2010.
- 691 Pearce, J.A., Harris, B.W., and Tindle, A.G.: Trace element discrimination diagrams for the
692 tectonic interpretation of granitic rocks, *Journal of Petrology*, 25, 956-983, 1984.
- 693 Peccerillo, A. and Taylor, S.R.: Geochemistry of Eocene calc–alkaline volcanic rocks from
694 the Kastamonu area, northern Turkey. *Contributions to Mineralogy and Petrology* 58,
695 63–81, 1976.
- 696 Plechov, P.Y., Tsai, A.E., Shcherbakov, V.D., and Dirksen, O.V.: Opacitization conditions of
697 hornblende in Bezmyannyi volcano andesites (March 30, 1956 eruption). *Petrology* 1,
698 19–35, 2008.
- 699 Rojay, B. and Süzen, L.: Tectonostratigraphic evolution of the Cretaceous dynamic basins on
700 accretionary ophiolitic melange prism, SW of Ankara Region, *Turkish Association of
701 Petroleum Geologists Bulletin*, 9, 1–12, 1997.
- 702 Rojay, B., Altiner, D., Altiner Özkan, S., Önen, A. P., James, S. and Thirlwall, M.F.:
703 Geodynamic significance of the Cretaceous pillow basalts from North Anatolian
704 Ophiolitic Mélange (Central Anatolia, Turkey): geochemical and paleontological
705 constraints. *Geodinamica Acta* 17/5, 349–361, 2004.
- 706 Saccani, E., Beccaluva, L., Photiades, A., and Zeda, O.: Petrogenesis and tectono–
707 magmatic significance of basalts and mantle peridotites from the Albanian–Greek
708 ophiolites and sub–ophiolitic mélanges. New constraints for the Triassic–Jurassic
709 evolution of the Neo–tethys in the Dinaride sector. *Lithos* 124, 227–242, 2011.

- 710 Sarifakioğlu, E., Dilek, Y., and Winchester, J.A.: Late Cretaceous Subduction Initiation and
711 Paleocene–Eocene Slab Breakoff Magmatism in South–Central Anatolia, Turkey,
712 *International Geology Review* 55 (1), 66–87, 2013.
- 713 Sarifakioğlu, E., Sevin, M., Esirtgen, E., Bilgiç, T., Duran, S., Parlak, O., Karabalık, N.,
714 Alemdar, S., Dilek, Y., and Uysal, I.: The geology of ophiolitic rocks around Çankırı–
715 Çorum Basen: petrogenesis, tectonics and ore deposits, Mineral Research and
716 Exploration Institute of Turkey (MTA) Report, No. 11449, 196 pp., 2011 (in Turkish,
717 unpublished).
- 718 Schiano, P., Clocchiatti, R., Shimizu, N., Mury, R.C., Johum, K.P., and Hofmann, A.W.:
719 Hydrous, silica rich melts in the subarc mantle and their relationship with erupted arc
720 lavas. *Nature* 377, 595–600, doi:10.1038/377595a0, 1995.
- 721 Shand, S.J.: *Eruptive Rocks*: London: Thomas Murby & Co, p. 1–360, 1927.
- 722 Shervais, J.W.: Ti–V plots and the petrogenesis of modern and ophiolitic lavas. *Earth and*
723 *Planetary Scientific Letters* 59, 101–118, 1982.
- 724 Sun, S.S. and McDonough, W.F.: Chemical and isotopic systematics of oceanic basalts:
725 Implications for mantle composition and processes. In: Saunders, A.D. and Norry, M.J.
726 (eds.), *Magmatism in the ocean basins*. Geological Society of London Special
727 Publication 42, 313–345, 1989.
- 728 Tankut, A., Dilek, Y. and Önen, P.: Petrology and geochemistry of the Neo–Tethyan
729 volcanism as revealed in the Ankara melange, Turkey. *Journal of Volcanology and*
730 *Geothermal Research* 85, 265–284, 1998.
- 731 Tatsumi, Y., Hamilton, D. and Nesbitt, R.W.: Chemical characteristics of fluid phase released
732 from a subducted lithosphere and origin of arc magmas. Evidence from high pressure
733 experiments and natural rocks. *Journal of Volcanology and Geothermal Research* 29,
734 293–309, 1986.
- 735 Tekeli, O.: Subduction complex of pre–Jurassic age, northern Anatolia, Turkey. *Geology* 9,
736 68–72, 1981.
- 737 Topuz, G., Altherr, R., Satır, M. and Schwarz, M.: Low grade metamorphic rocks from the
738 Pular complex, NE Turkey: Implications for pre–Liassic evolution of the Eastern

- 739 Pontides. *International Journal of Earth Sciences* 93, p. 72–91, doi:10.1007/s00531–
740 003–0372–5, 2004.
- 741 Topuz, G., Okay, A.I., Altherr, R., Meyer, H.P. and Nasdala, L.: Partial high–pressure
742 aragonitization of micritic limestones in an accretionary complex, Tavşanlı Zone, NW
743 Turkey. *Journal of Metamorphic Geology* 24, p. 603–613, 2006.
- 744 Tüysüz, O., Dellaloğlu, A.A. and Terzioğlu, N.: A magmatic belt within the Neo–tethyan
745 suture zone and its role in the tectonic evolution of northern Turkey. *Tectonophysics*
746 243, 173–191, 1995.
- 747 Uğuz, M. F., Sevin, M. and Duru, M.: 1/500 000 scale geological maps of Turkey, Sinop
748 Quadrangle (MTA General Directorate, Ankara), 2002.
- 749 White, W.M.: Sources of oceanic basalts: radiogenic isotopic evidence. *Geology* 13, 115–
750 118, 1985.
- 751 Whitney, D.L., and Dilek, Y.: Metamorphism during crustal thickening and extension in
752 central Anatolia: The Nigde metamorphic core complex. *Journal of Petrology* 39, 1385–
753 1403, 1998.
- 754 Wood, D.A.: The application of a Th–Hf–Ta diagram to problems of tectonomagmatic
755 classification and to establishing the nature of crustal contamination of basaltic lavas of
756 the British Tertiary Volcanic Province. *Earth and Planet Scientific Letters* 56, 11–30,
757 1980.
- 758 Zindler, A. and Hart, S.R.: Chemical geodynamics. *Annual Review of Earth and Planet*
759 *Science Letters* 14, 493–571, 1986.
- 760

761 **FIGURE CAPTIONS**

762 **Figure 1.** Simplified ophiolite map of Turkey showing the distribution of the suture zones and
763 some of the major tectonic entities in Turkey (from MTA, 2001). The inset box refers to the
764 map area in Fig. 2.

765 **Figure 2.** Geological map of the Çankırı–Çorum area along the IAESZ in north-central
766 Turkey (modified after Uğuz et al., 2002). NAF: North Anatolian Fault.

767 **Figure 3.** Geological map of the Kalecik area, east of Ankara, showing the distribution of the
768 ophiolitic, turbiditic and island-arc rock units in the Ankara Mélange in north-central Turkey.

769 **Figure 4.** Geological map of the northern part of the Kalecik area (modified after Hakyemez
770 et al., 1986).

771 **Figure 5.** View of the Ankara Mélange and the Karakaya Complex (Sakarya Continent). Key
772 to lettering: AOM = Ankara Mélange, β = basalt, KC = Karakaya Complex, ms = mudstone,
773 pg = plagiogranite, sp = serpentinized peridotites.

774 **Figure 6.** Simplified geological map of the Yapraklı–Çankırı area, showing the distribution of
775 the ~180 Ma Neotethyan ophiolitic units, ophiolitic mélange and island-arc rocks.

776 **Figure 7.** Geological map of the Laloglu (Çorum) area, showing the Neotethyan Eldivan
777 ophiolite and the island-arc rock units.

778 **Figure 8.** (a) Neritic limestone covering the seamount volcanic-volcaniclastic rocks in the
779 Ankara Mélange. (b) Seamount pillow lavas in the Ankara Mélange. NL= neritic limestone.

780 **Figure 9.** (a) Limestone-volcanic sandstone intercalation in the island-arc sequence. (b) A
781 mafic dike (island-arc origin) crosscutting the pelagic limestone rocks. (c) Alkaline basaltic
782 rocks with columnar joint structures. (d) Arc volcaniclastic rocks intruded by basaltic to
783 andesitic dikes.

784 **Figure 10.** (a) Upper Cretaceous reefal limestone with rudist fossils unconformably overlying
785 the arc volcanic rocks. (b) Reefal limestone underlain by volcanic sandstone. (c) Alkaline
786 pillow lavas overlain by volcanic sandstone-pebblestone. (d) Alkaline pillow lavas with radial
787 joint structures. All rocks in a through d represent the island-arc units.

788 **Figure 11.** Lamprophyric dikes crosscutting various lithological units in the Ankara Mélange.

789 **Figure 12.** Photomicrographs of (a) A seamount alkaline basalt sample. (b) Doleritic dike
790 rock of the 180 Ma Neotethyan oceanic crust. (c) Island-arc alkaline basalt sample in cross-
791 polarized light. (d) Island-arc alkaline basalt sample in plane-polarized light. (e) Island-arc
792 basaltic andesite dike, showing a glomeroporphyritic texture. (f) Lamprophyric dike rock with
793 small prismatic cpx (diopside) in a feldspar + phlogopite groundmass (plane-polarized light).
794 (g). Lamprophyric dike rock with small prismatic cpx (diopside and phlogopite). (h) Syeno-
795 dioritic pluton rock with plagioclase (altered to clay minerals) and biotite + hornblende and
796 minor cpx (cross-polarized light).

797 **Figure 13.** Geochemical classification of ophiolitic and seamount volcanic rocks. (a) Total
798 alkali vs. SiO₂ diagram (Le Bas et al., 1986). (b) AFM diagram (Irvine and Baragar, 1971). (c)
799 Ti–Zr–Y discrimination diagram (Pearce and Cann, 1973). (d) Ti–V diagram (Shervais,
800 1982). (e) N-MORB-normalized multi-element diagrams of the most representative samples
801 (normalization values from Sun and McDonough, 1989). Key to lettering: A = andesite, B =
802 basalt, BA = basaltic andesite, BS = basanite, BTA = basaltic trachyandesite, D = dacite, F =
803 foidite, PC = picobasalt, PH = phonolite, PHTP = phonotephrite, R = rhyolite, T = trachyte,
804 TA = trachyandesite, TB = trachybasalt, TD = trachydacite, TP = tephrite. IB = alkali-
805 subalkali subdivision from Irvine and Baragar (1971). .

806 **Figure 14.** Geochemical classification of island-arc rocks. (a) Total alkali vs. SiO₂ diagram
807 (Le Bas et al., 1986). (b) TAS diagram (Cox et al., 1979) for syeno-dioritic pluton rocks. (c)
808 Alk–MgO–FeO_t diagram (Irvine and Baragar, 1971) of the subalkaline arc volcanic units
809 (Dönmez et al., 2009, and this study). (d) K₂O vs. SiO₂ diagram (Peccerillo and Taylor,
810 1976). (e) Th vs. Co diagram (Hastie et al., 2007). Ce/Yb vs. Ta/Yb diagram (Pearce, 1982).

811 **Figure 15.** Major oxides and trace elements vs. MgO variation diagrams for various alkaline
812 island-arc units.

813 **Figure 16.** (a) A/CNK, molar Al₂O₃/(CaO+Na₂O+K₂O) vs. A/NK, molar Al₂O₃/(Na₂O+K₂O)
814 diagram (Shand, 1927). (b, c) trace element discrimination diagrams (Nb–Y and Rb vs.
815 Y+Nb) for syenodioritic pluton rocks (fields from Pearce et al., 1984; VAG = volcanic arc
816 granites, WPG = within-plate granites, ORG = ocean ridge granites. SYN-COLG = syn-
817 collisional granites. (d) Ti–Zr–Y diagram. (e) Ti–V diagram. (f) TiO₂ vs. Al₂O₃ diagram. (g) Y
818 vs. Zr diagram. (h) Th/Yb vs. Nb/Yb diagram (fields after Pearce and Cann, 1973; Shervais,
819 1982; Muller et al., 1992; Pearce, 2008).

820 **Figure 17.** (a) Primitive mantle-normalized multi-element diagrams for the high-K shoshonitic
821 arc rocks (normalization values from Sun & McDonough, 1989). (b) Chondrite-normalized
822 REE patterns of the same rocks (normalization values from Sun & McDonough, 1989).

823 **Figure 18.** (a) Ba/Nb vs. La/Nb diagram for the high-K island arc rocks. The data for N-
824 MORB, OIB and PM are from Sun & McDonough (1989). (b) La/Yb vs. La diagram for the
825 island-arc rock units, illustrating the effects of partial melting and fractionation in their melt
826 evolution.

827 **Figure 19.** Isotope variation diagrams for the Upper Cretaceous–Lower Paleocene high-K
828 island-arc rocks. (a) $^{143}\text{Nd}/^{144}\text{Nd}$ vs. $^{87}\text{Sr}/^{86}\text{Sr}$ diagram. (b) $^{206}\text{Pb}/^{204}\text{Pb}$ vs. $^{208}\text{Pb}/^{204}\text{Pb}$ diagram.
829 (c) $^{206}\text{Pb}/^{204}\text{Pb}$ vs. $^{207}\text{Pb}/^{204}\text{Pb}$ diagram. (d) $^{87}\text{Sr}/^{86}\text{Sr}$ vs. $^{206}\text{Pb}/^{204}\text{Pb}$ diagram. (e) $^{143}\text{Nd}/^{144}\text{Nd}$
830 vs. $^{206}\text{Pb}/^{204}\text{Pb}$ diagram. Compositional fields for the upper and lower crust, MORB (mid-
831 ocean ridge basalt), HIMU (enriched mantle in U and Th relative to Pb), OIB (ocean island
832 basalt), EMI (enriched mantle I) and EMII (enriched mantle II) are from Zindler and Hart
833 (1986). The field for *Oceanic Islands* is from White (1985). NHRL = Northern Hemisphere
834 Reference Line.

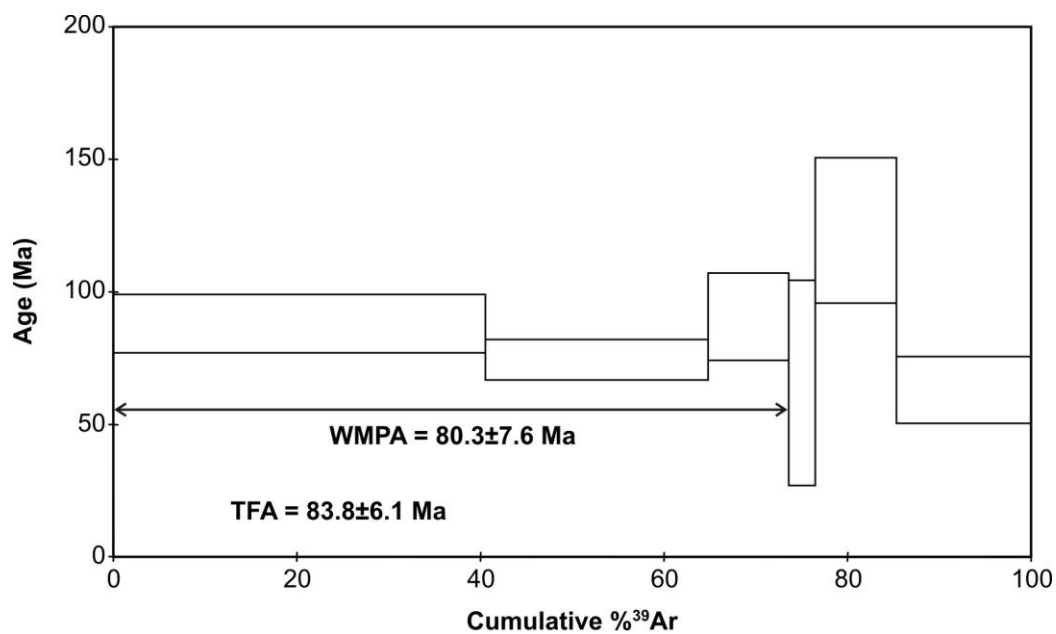
835 **Figure 20.** Sequential tectonic diagrams depicting the intra-oceanic magmatic evolution of
836 the Ankara Mélange in the Northern Neotethys during the Jurassic – Paleocene. A.
837 Suprasubduction zone generation of the oldest Neotethyan oceanic crust (~180 Ma) in the
838 upper plate of a North-dipping intra-oceanic subduction zone, and seamount construction
839 (SM1 and SM2) in the downgoing oceanic plate. High-grade metamorphic rock blocks and
840 turbiditic sandstone-mudstone sequences in the Ankara Mélange formed in the subduction
841 channel (blue in color) and the accretionary prism, respectively. B. Accretion of Seamount-1
842 into the accretionary complex and related deformation in the subduction-accretion system. C.
843 Slab rollback and associated extension and SSZ oceanic crust formation (~85-80 Ma) in the
844 upper plate. Accretion of Seamount-2 into the accretionary complex, and the lateral growth
845 and deformation in the subduction-accretion system. D. Island arc construction and
846 magmatism on and across the pre-existing SSZ oceanic lithosphere and the subduction-
847 accretion complex (i.e. Ankara Mélange units). With continued slab retreat, arc magmatism
848 shifts southward following the migrating trench, and becomes more alkaline in time,
849 producing lamprophyric and syeno-dioritic intrusions. See text for further explanation.

850 TABLES

851 Table 1. Whole-rock $^{40}\text{Ar}/^{39}\text{Ar}$ age data for a basaltic rock sample (YK-11) from the youngest SSZ ophiolite in the Ankara Mélange, Turkey.**Sample: YK-11 (whole rock): Basalt, $J=0.004426\pm 0.000051$**

T°C	$^{40}\text{Ar}/^{39}\text{Ar}$ (STP)	$^{40}\text{Ar}/^{39}\text{Ar}$	$\pm 1\sigma$	$^{38}\text{Ar}/^{39}\text{Ar}$	$\pm 1\sigma$	$^{37}\text{Ar}/^{39}\text{Ar}$	$\pm 1\sigma$	$^{36}\text{Ar}/^{39}\text{Ar}$	$\pm 1\sigma$	Ca/K	$\sum^{39}\text{Ar}$ (%)	Age (Ma)	$\pm 1\sigma$	$\pm 1\sigma$
500	20.81×10^{-9}	29.6	0.1	0.0418	0.0029	0.479	0.011	0.0620	0.0049	1.72	40.5	88.0	11.0	
600	9.45×10^{-9}	22.5	0.1	0.0364	0.0037	0.584	0.011	0.0438	0.0033	2.10	64.8	74.4	7.6	
700	12.18×10^{-9}	79.8	0.6	0.0733	0.0129	0.627	0.036	0.2306	0.0075	2.26	73.6	90.6	16.5	
800	9.18×10^{-9}	184.7	9.4	0.1457	0.0530	0.751	0.145	0.5966	0.0347	2.70	76.5	65.7	38.7	
1000	9.00×10^{-9}	58.5	0.7	0.0714	0.0153	1.630	0.046	0.1440	0.0125	5.87	85.3	123.2	27.4	
1130	8.12×10^{-9}	32.0	0.2	0.0332	0.0070	1.131	0.019	0.0811	0.0055	4.07	100.0	62.9	12.6	

Age Spectrum: The sample yielded age spectrum with well behaved plateau, characterized by 73.6% of ^{39}Ar , Age value of 80.3 ± 7.6 Ma. On the Inverse Isochrone Plot points form linear regression characterized by age value of 75.8 ± 7.4 and $(^{40}\text{Ar}/^{36}\text{Ar})_0 = 300 \pm 8$

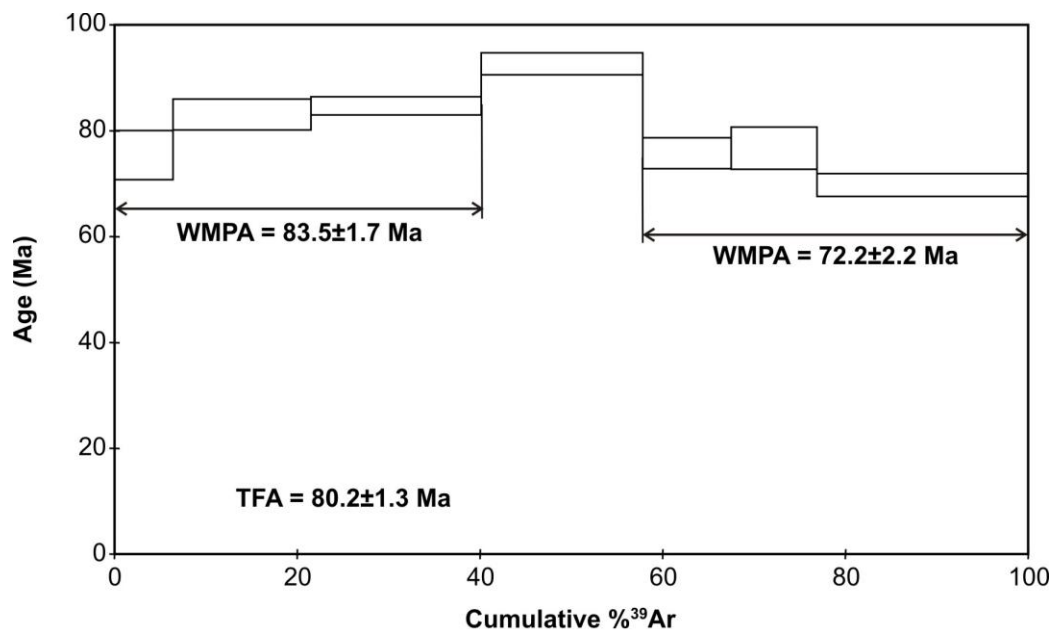


852 **Table 2a.** Whole-rock $^{40}\text{Ar}/^{39}\text{Ar}$ age data for an epidote-glaucophane schist rock from a metamorphic block in the Ankara Mélange, Turkey.

Sample: YK-6: epidote-glaucophane schist, $J=0.004420\pm0.000051$

T°C	$^{40}\text{Ar}_{\text{cc}}$ (STP)	$^{40}\text{Ar}/^{39}\text{Ar}$	$\pm 1\sigma$	$^{38}\text{Ar}/^{39}\text{Ar}$	$\pm 1\sigma$	$^{37}\text{Ar}/^{39}\text{Ar}$	$\pm 1\sigma$	$^{36}\text{Ar}/^{39}\text{Ar}$	$\pm 1\sigma$	Ca/K	$\sum^{39}\text{Ar}$ (%)	Age (Ma)	$\pm 1\sigma$	$\pm 1\sigma$
500	35.70×10^{-9}	48.05	0.1	0.0463	0.003	1.5385	0.0082	0.1299	0.002	5.54	6.4	75.4	4.6	
600	32.83×10^{-9}	18.75	0.02	0.0257	0.0005	1.221	0.0031	0.0274	0.0012	4.4	21.5	83.1	2.9	
700	38.21×10^{-9}	17.65	0.01	0.0255	0.0007	0.5962	0.0014	0.0229	0.0006	2.15	40.1	84.7	1.7	
800	40.74×10^{-9}	19.89	0.02	0.0236	0.001	1.3996	0.0017	0.027	0.0008	5.04	57.8	92.7	2.1	
900	21.78×10^{-9}	19.32	0.03	0.0277	0.0008	10.821	0.0144	0.0325	0.0012	38.96	67.5	75.8	2.9	
1000	16.15×10^{-9}	14.81	0.03	0.0253	0.0016	12.5237	0.0228	0.0168	0.0017	45.09	76.9	76.8	4	
1130	35.36×10^{-9}	13.2	0.01	0.0244	0.0004	9.9743	0.0097	0.0145	0.0009	35.91	100	69.8	2.2	

Age Spectrum: The sample yielded age spectrum with two 3 steps plateaus, characterized accordingly by 40.1% of ^{39}Ar , Age value of 83.5 ± 1.7 Ma and 42.2 % of ^{39}Ar , Age value of 72.2 ± 2.2 Ma. On the Inverse Isochrone Plot points form two linear regression characterized by age value of 87.8 ± 2.5 and $(^{40}\text{Ar}/^{36}\text{Ar})_0 = 285 \pm 5$. The presence of two age plateaus evidence to isotope heterogeneity of YK 6.

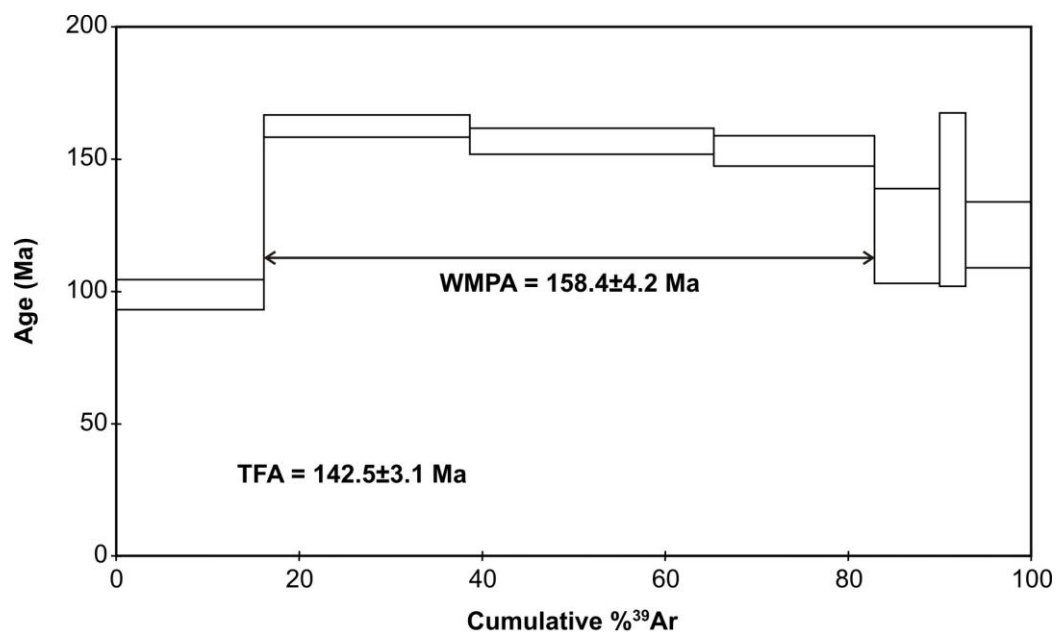


853 **Table 2b.** Whole-rock $^{40}\text{Ar}/^{39}\text{Ar}$ age data for an epidote-chlorite schist rock from a metamorphic block in the Ankara Mélange, Turkey.

Sample: YK-7: epidote-chlorite schist, $J=0.004121\pm0.000044$

T°C	$^{40}\text{Ar}_{\text{cc}}$ (STP)	$^{40}\text{Ar}/^{39}\text{Ar}$	$\pm 1\sigma$	$^{38}\text{Ar}/^{39}\text{Ar}$	$\pm 1\sigma$	$^{37}\text{Ar}/^{39}\text{Ar}$	$\pm 1\sigma$	$^{36}\text{Ar}/^{39}\text{Ar}$	$\pm 1\sigma$	Ca/K	$\sum^{39}\text{Ar}$ (%)	Age (Ma)	$\pm 1\sigma$	$\pm 1\sigma$
500	33.53×10^{-9}	57.6	0.2	0.051	0.0027	4.4795	0.0134	0.1488	0.0027	16.13	16.1	98.8	5.7	
600	31.15×10^{-9}	38.4	0.1	0.0304	0.0018	3.5391	0.0081	0.0525	0.0019	12.74	38.7	162.5	4.2	
700	42.75×10^{-9}	44.5	0.1	0.0355	0.0018	5.4612	0.0142	0.0761	0.0023	19.66	65.3	156.8	4.9	
800	19.66×10^{-9}	31	0.1	0.0271	0.0028	1.8875	0.0089	0.0323	0.0027	6.8	82.9	153.1	5.8	
900	12.92×10^{-9}	50.5	0.4	0.0507	0.0062	3.436	0.0365	0.1139	0.0087	12.37	90	121	17.9	
1000	6.24×10^{-9}	60.7	1	0.0518	0.0203	11.168	0.1806	0.1419	0.0162	40.2	92.8	134.7	32.7	
1130	22.81×10^{-9}	88.4	0.5	0.0743	0.0064	56.2813	0.3389	0.2421	0.0062	202.61	100	121.4	12.4	

Age Spectrum: The sample yielded age spectrum with 3 steps plateau, characterized by 66.7% of ^{39}Ar , Age value of 158.4 ± 4.2 Ma. On the Inverse Isochrone Plot points form linear regression characterized by age value of 166.9 ± 5.9 and $(^{40}\text{Ar}/^{36}\text{Ar})_0 = 272 \pm 8$.

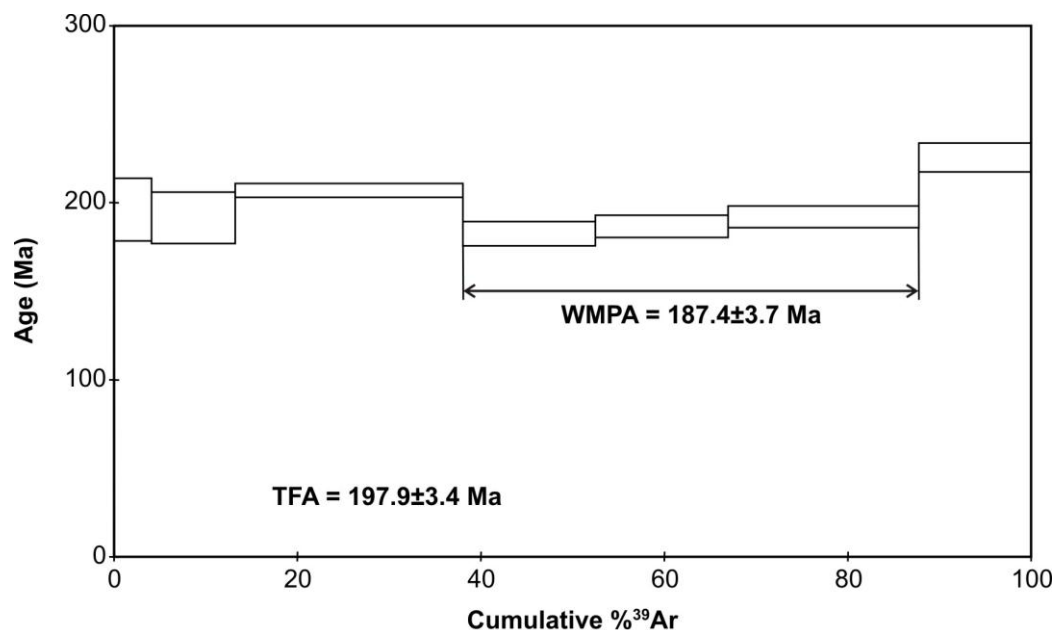


855 **Table 2c.** Whole-rock $^{40}\text{Ar}/^{39}\text{Ar}$ age data for an epidote-actinolite schist rock from a metamorphic block in the Ankara Mélange, Turkey.

Sample: YK-1: epidote-actinolite schist, $J=0.004428\pm0.000051$

T°C	$^{40}\text{Ar}_{\text{cc}}$ (STP)	$^{40}\text{Ar}/^{39}\text{Ar}$	$\pm 1\sigma$	$^{38}\text{Ar}/^{39}\text{Ar}$	$\pm 1\sigma$	$^{37}\text{Ar}/^{39}\text{Ar}$	$\pm 1\sigma$	$^{36}\text{Ar}/^{39}\text{Ar}$	$\pm 1\sigma$	Ca/K	$\Sigma^{39}\text{Ar}$ (%)	Age (Ma)	$\pm 1\sigma$	$\pm 1\sigma$
500	28.20×10^{-9}	195.111	1.614	0.1185	0.0072	8.7082	0.0754	0.5725	0.0095	31.35	4.1	196.1	17.7	
600	35.22×10^{-9}	109.08	0.736	0.0809	0.0035	12.8319	0.0878	0.2835	0.007	46.19	13.2	191.6	14.5	
700	46.14×10^{-9}	52.526	0.083	0.0345	0.0021	5.2249	0.0101	0.0848	0.0016	18.81	38.1	207	4	
800	22.10×10^{-9}	43.305	0.132	0.032	0.0025	3.3143	0.0128	0.0652	0.003	11.93	52.5	182.5	6.8	
900	28.97×10^{-9}	56.607	0.158	0.0384	0.0023	16.1294	0.0458	0.1083	0.0028	58.07	67	186.6	6.3	
1000	30.80×10^{-9}	41.871	0.112	0.0328	0.0018	21.4028	0.0573	0.0558	0.0027	77.05	87.8	192.1	6	
1130	30.24×10^{-9}	69.813	0.261	0.0523	0.0025	34.5698	0.1292	0.1345	0.0038	124.45	100	225.6	8.2	

Age Spectrum: The sample yielded age spectrum with 3 steps plateau, characterized by 50% of ^{39}Ar , Age value of 187.4 ± 3.7 Ma. On the Inverse Isochrone Plot one can observe linear regression characterized by age value of 166.1 ± 12.3 .



857 **Table 3.** Whole-rock K/Ar age data from metamorphic rock blocks in the Ankara Mélange, Turkey.

Sample no.	Rock	%K	40Ar/36Ar	⁴⁰Ar_{rad}, nl/g	% ⁴⁰Ar_{air}	error	Age, Ma
CE.981	Phyllite	1.68	883.2	7.932	33.5	4.5	119.8±3.3
CE.228	Actinolite schist	0.36	347.8	2.558	85.1	0.6	177.4±5.8
CE.976	Amphibole-epidote schist	0.22	405.9	2.316	72.9	1.3	256.9±8.0

858

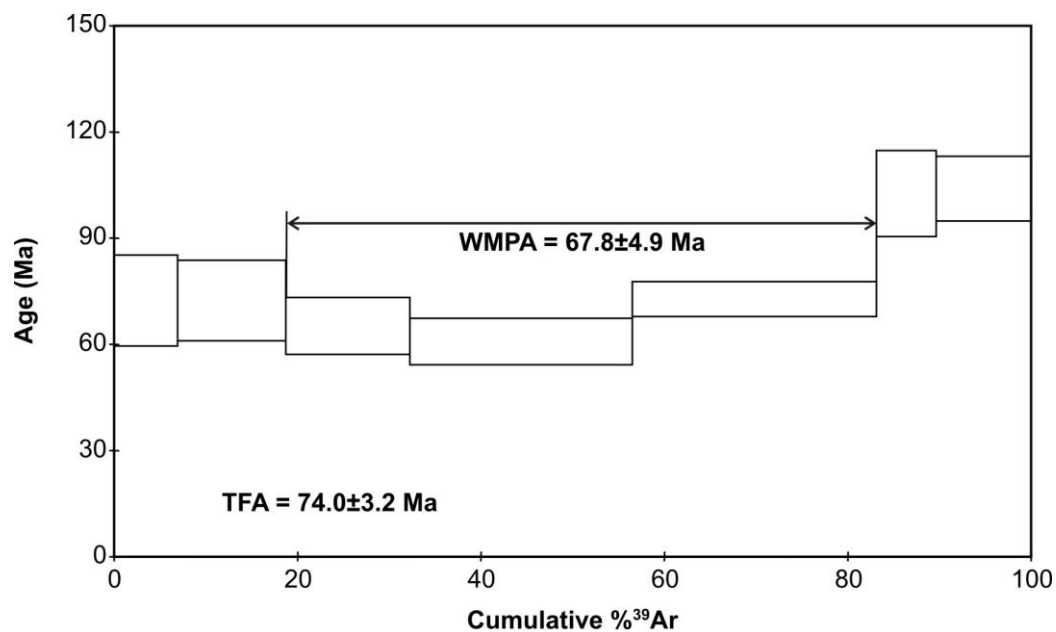
859

860 **Table 4a.** Whole-rock $^{40}\text{Ar}/^{39}\text{Ar}$ age data for an island-arc basaltic rock (Sample No. YK-4) in the Ankara Mélange, Turkey.

Sample: YK-4 (whole rock): Basalt, $J=0.004353\pm0.000050$

T°C	$^{40}\text{Ar}_{\text{cc}}$ (STP)	$^{40}\text{Ar}/^{39}\text{Ar}$	$\pm 1\sigma$	$^{38}\text{Ar}/^{39}\text{Ar}$	$\pm 1\sigma$	$^{37}\text{Ar}/^{39}\text{Ar}$	$\pm 1\sigma$	$^{36}\text{Ar}/^{39}\text{Ar}$	$\pm 1\sigma$	Ca/K	$\Sigma^{39}\text{Ar}$ (%)	Age (Ma)	$\pm 1\sigma$
500	44.60×10^{-9}	168.69	0.97	0.1269	0.007	7.5932	0.0458	0.539	0.0065	27.34	6.9	72.4	12.8
600	14.83×10^{-9}	32.9	0.17	0.0413	0.0033	10.1845	0.0528	0.0795	0.0051	36.66	18.7	72.4	11.4
700	13.82×10^{-9}	26.82	0.1	0.0333	0.0048	4.2753	0.017	0.0621	0.0036	15.39	32.2	65.2	8
800	24.70×10^{-9}	26.65	0.08	0.0331	0.0022	1.935	0.0067	0.0635	0.0029	6.97	56.5	60.8	6.6
900	18.59×10^{-9}	18.29	0.04	0.021	0.0013	1.3887	0.0051	0.0299	0.0022	5	83.1	72.8	4.9
1000	7.83×10^{-9}	31.49	0.17	0.0381	0.0053	1.4804	0.0211	0.0611	0.0055	5.33	89.7	102.6	12.1
1130	11.68×10^{-9}	29.58	0.12	0.0279	0.0033	3.5167	0.016	0.054	0.0041	12.66	100	104	9.2

Age Spectrum: The sample yielded age spectrum with 3 steps plateau, characterized by 64.4% of ^{39}Ar , Age value of 67.8 ± 4.9 Ma. On the Inverse Isochrone Plot points form linear regression characterized by age value of 68.1 ± 4.4 and $(^{40}\text{Ar}/^{36}\text{Ar})_0 = 296.1 \pm 3.5$.



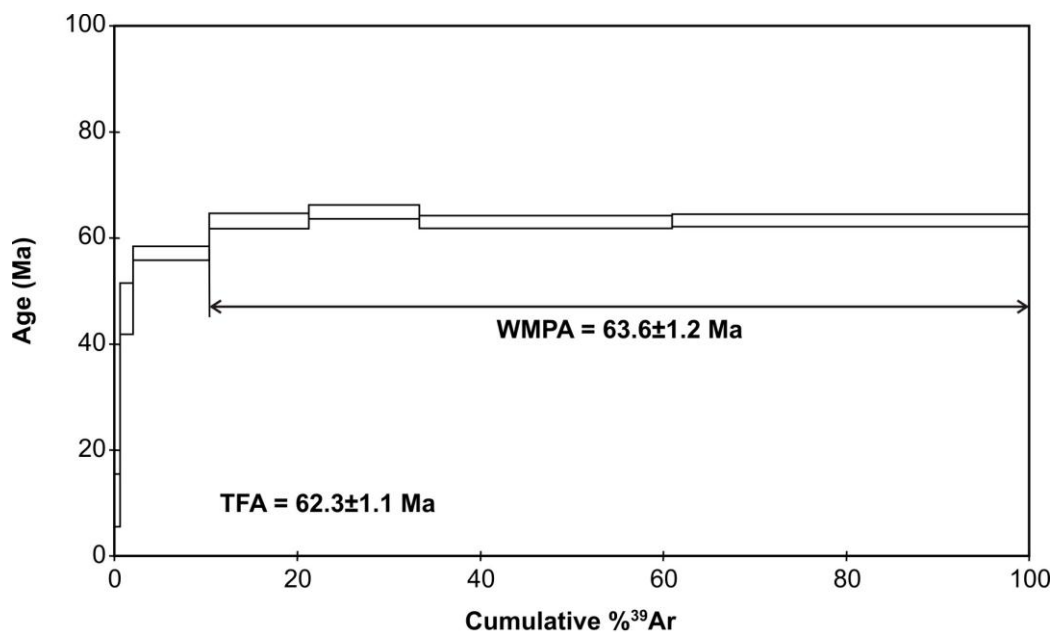
861

862 **Table 4b.** $^{40}\text{Ar}/^{39}\text{Ar}$ biotite age data for a lamprophyre dike (Sample No. YK-19) from the island-arc unit in the Ankara Mélange, Turkey.

Sample: YK-19 (biotite): Lamprophyre, $J=0.007143 \pm 0.000133$

T°C	$^{40}\text{Ar}_{\text{cc}}$ (STP)	$^{40}\text{Ar}/^{39}\text{Ar}$	$\pm 1\sigma$	$^{38}\text{Ar}/^{39}\text{Ar}$	$\pm 1\sigma$	$^{37}\text{Ar}/^{39}\text{Ar}$	$\pm 1\sigma$	$^{36}\text{Ar}/^{39}\text{Ar}$	$\pm 1\sigma$	Ca/K	$\sum^{39}\text{Ar}$ (%)	Age (Ma)	$\pm 1\sigma$
500	3.9×10^{-9}	92.802	0.0393	0.015480	0.004274	0.61970	0.05770	0.028643	0.001314	22.30	0.6	10.50	5.0
625	7.7×10^{-9}	83.584	0.0116	0.015744	0.001217	0.31455	0.01480	0.015871	0.001284	1.13	2.0	46.7	4.80
750	37.9×10^{-9}	69.914	0.0044	0.013301	0.000117	0.05874	0.00360	0.008418	0.000210	0.21	10.40	57.1	1.30
850	45.7×10^{-9}	64.526	0.0017	0.013498	0.000076	0.04725	0.00102	0.004948	0.000237	0.17	21.20	63.2	1.40
950	51.6×10^{-9}	65.506	0.0033	0.013393	0.000248	0.08738	0.00394	0.004805	0.000142	0.31	33.3	64.9	1.30
1050	112.6×10^{-9}	62.462	0.0035	0.013738	0.000060	0.07037	0.00091	0.004305	0.000083	0.25	61.0	63.0	1.20
1130	156.9×10^{-9}	61.778	0.0020	0.013593	0.000030	0.07395	0.00067	0.003986	0.000051	0.27	100.0	63.3	1.20

Age Spectrum: The sample yielded age spectrum with four steps Plateau characterized by 89.6% of ^{39}Ar , Age value of 63.6 ± 1.2 Ma. On the Inverse Isochrone Plot plateau points form linear trend, characterized by age value of 57.5 ± 4.1 Ma, MSWD = 1.5



863

864

Table 4c. Whole-rock $^{40}\text{Ar}/^{39}\text{Ar}$ age data for a lamprophyre dike (Sample No. YK-20) from the island-arc unit in the Ankara Mélange, Turkey.**Sample: YK-20 (whole rock): Lamprophyre, $J=0.007258 \pm 0.000137$**

T°C	$^{40}\text{Ar}_{\text{cc}}$ (STP)	$^{40}\text{Ar}/^{39}\text{Ar}$	$\pm 1\sigma$	$^{38}\text{Ar}/^{39}\text{Ar}$	$\pm 1\sigma$	$^{37}\text{Ar}/^{39}\text{Ar}$	$\pm 1\sigma$	$^{36}\text{Ar}/^{39}\text{Ar}$	$\pm 1\sigma$	Ca/K	$\sum^{39}\text{Ar}$ (%)	Age (Ma)	$\pm 1\sigma$	$\pm 1\sigma$
550	114.7×10^{-9}	48.724	0.0048	0.014063	0.000040	0.28860	0.00023	0.004714	0.000071	1.04	16.20	45.0	0.9	
625	78.3×10^{-9}	71.168	0.0064	0.014657	0.000137	128.516	0.00083	0.006715	0.000045	4.63	23.70	66.0	1.20	
700	73.1×10^{-9}	63.482	0.0041	0.014148	0.000062	115.422	0.00187	0.003713	0.000142	4.16	31.70	67.5	1.40	
775	85.2×10^{-9}	62.554	0.0032	0.013660	0.000068	0.51460	0.00080	0.003174	0.000096	1.85	41.0	68.3	1.30	
850	68.1×10^{-9}	59.659	0.0028	0.013744	0.000112	0.19993	0.00023	0.004958	0.000090	0.72	48.9	58.0	1.10	
950	54.6×10^{-9}	58.431	0.0024	0.014092	0.000162	0.29838	0.00075	0.004897	0.000152	1.07	55.3	56.7	1.20	
1050	210.7×10^{-9}	50.825	0.0020	0.013886	0.000024	0.61827	0.00022	0.005145	0.000055	2.23	83.8	46.0	0.9	
1130	121.2×10^{-9}	51.432	0.0013	0.014028	0.000073	144.061	0.00118	0.005433	0.000056	5.19	100.0	45.7	0.9	

Age Spectrum: The sample yielded complex age spectrum with noticeable hump after low temperature step containing three steps intermediate plateau followed by high temperature two steps intermediate Plateau. Intermediate plateaus are characterized accordingly by 24.8% of ^{39}Ar , Age value of 67.2 ± 1.2 Ma and 44.7% of ^{39}Ar , Age value of 45.9 ± 0.9 Ma.

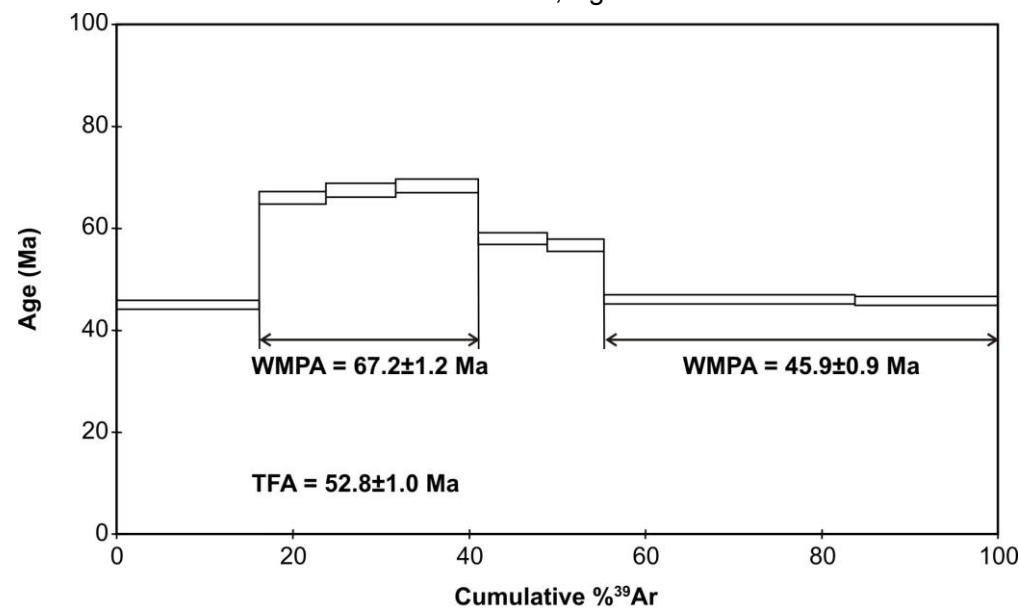
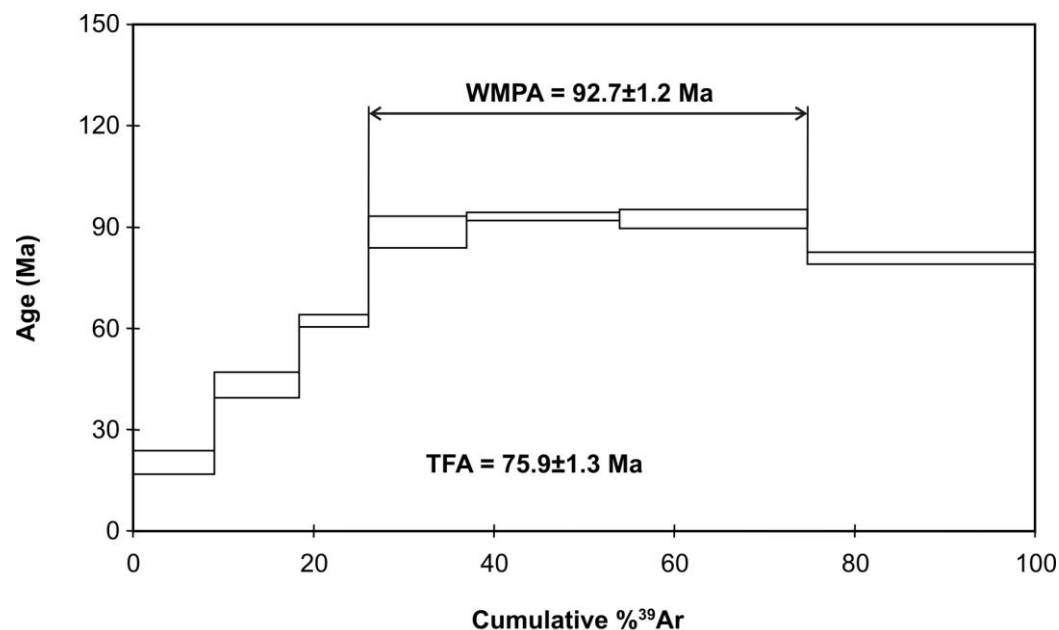


Table 4d. $^{40}\text{Ar}/^{39}\text{Ar}$ biotite age data for a syeno-diorite plutonic rock (Sample No. YK-438) from the island-arc unit in the Ankara Mélange, Turkey.**Sample: YK-438 (biotite): Syeno-diorite, $J=0.004553 \pm 0.000054$**

T°C	$^{40}\text{Ar}_{\text{cc}}$ (STP)	$^{40}\text{Ar}/^{39}\text{Ar}$	$\pm 1\sigma$	$^{38}\text{Ar}/^{39}\text{Ar}$	$\pm 1\sigma$	$^{37}\text{Ar}/^{39}\text{Ar}$	$\pm 1\sigma$	$^{36}\text{Ar}/^{39}\text{Ar}$	$\pm 1\sigma$	Ca/K	$\sum^{39}\text{Ar}$ (%)	Age (Ma)	$\pm 1\sigma$	$\pm 1\sigma$
500	10.2×10^{-9}	61.084	0.0090	0.01989	0.00107	0.7800	0.0026	0.01226	0.00144	2.81	9.0	20.30	3.46	
600	14.4×10^{-9}	82.535	0.0136	0.01627	0.00075	15.022	0.0075	0.00992	0.00159	5.41	18.4	43.20	3.79	
700	17.3×10^{-9}	121.050	0.0098	0.00960	0.00130	21.617	0.0064	0.01488	0.00069	7.78	26.1	62.22	1.78	
800	25.9×10^{-9}	128.671	0.0263	0.01743	0.00152	0.9964	0.0146	0.00617	0.00198	3.59	37.0	88.51	4.68	
900	39.8×10^{-9}	126.457	0.0087	0.01645	0.00019	0.8052	0.0025	0.00343	0.00027	2.9	53.9	93.11	1.25	
1000	48.8×10^{-9}	126.405	0.0147	0.01668	0.00067	0.4739	0.0055	0.00371	0.00111	1.71	74.8	92.41	2.77	
1130	52.0×10^{-9}	111.241	0.0102	0.01900	0.00068	21.389	0.0021	0.00361	0.00065	7.7	100.0	80.77	1.78	

Age Spectrum: The sample yielded age spectrum with three steps plateau characterized by 48.6 % of ^{39}Ar , Age value of 92.7 ± 1.2 Ma. On the Inverse Isochrone Plot points don't form linear regression.



867 **Table 5.** Major, trace element and REE data for a selected group of volcanic and dike rocks
868 from the Neotethyan ophiolitic units in the Ankara Mélange (first nine samples from Tankut et
869 al., 1998).

Sample no	BM1	BM3	BM5	95GK4	95GK6	95GKE4	96GKE51	96GKE57	96GKE58B	CE.07	CE.08
Rock-type	Basalt	Basaltic andesite	Basalt	Dolerite	Dolerite	Dolerite	Dolerite	Dolerite	Dolerite	Basalt	Basalt
Oxide, wt %											
SiO ₂	50.53	51.34	50.47	51.08	49.45	51.53	48.93	50.45	47.08	55.50	54.94
TiO ₂	1.12	0.26	1.13	1.66	1.68	1.82	0.67	1.74	1.55	0.82	0.81
Al ₂ O ₃	15.96	17.16	15.93	13.45	13.52	12.53	11.00	12.97	11.18	18.43	18.66
Fe ₂ O ₃	10.01	6.80	9.99	11.91	13.23	12.69	9.07	12.31	12.21	8.12	8.47
MnO	0.14	0.12	0.14	0.23	0.22	0.23	0.18	0.23	0.22	0.60	0.63
MgO	6.32	8.17	5.89	7.04	6.41	6.67	10.54	6.30	8.67	3.54	3.81
CaO	4.88	11.07	5.33	9.18	10.91	7.93	15.30	8.66	13.11	1.27	1.17
Na ₂ O	3.31	2.30	3.34	3.79	2.89	3.89	0.43	3.41	1.22	7.62	7.50
K ₂ O	0.28	0.28	0.29	0.34	0.36	0.39	0.07	0.37	0.12	0.17	0.19
P ₂ O ₅	0.13	0.07	0.12	0.17	0.21	0.22	0.06	0.21	0.23	0.09	0.10
LOI	6.81	2.05	6.94	1.2	1.04	0.85	3.12	1.69	3.06	3.70	3.50
Total	99.49	99.62	99.57	100.05	99.92	99.75	99.35	98.34	98.65	99.85	99.84
Trace, ppm											
Cr	53.00	166.00	36.00	70.00	84.00	130.00	624.00	134.00	103.00	27.40	20.55
Ni	10.00	101.00	8.00	21.00	25.00	48.00	91.00	59.00	37.00	13.20	11.70
Co										27.90	26.10
Sc				35	38	32	41	35	45		
Rb	11.00	9.00	12.00	4.00	4.00	5.00	2.00	7.00	0.00	2.10	2.40
Ba	242.00		270.00	60.00	503.00	188.00	22.00	185.00	52.00	130.00	110.00
Sr	441.00	100.00	420.00	174.00	510.00	402.00	24.00	208.00	71.00	472.80	494.80
Cs							0.64	24.94	3.91	0.40	0.50
Th	0.47	0.60	0.44	0.00	1.00	3.00	2.00	4.00	3.00	0.60	0.60
U				0.21	0.26	0.29	0.14	0.28	0.28	0.30	0.30
Nb	3.00	2.60	4.00	3.70	5.70	4.00	1.30	3.40	4.80	1.30	1.40
Ta	0.00	0.00	0.00	0.24	0.29	0.25	0.15	0.18	0.29	0.10	0.10
Zr	96.00	21.00	98.00	101.00	126.00	119.00	39.00	91.00	113.00	37.90	43.60
Hf	1.70	0.30	2.20	2.77	3.10	3.14	1.16	2.64	3.13	1.40	1.40
Y	25.00	7.00	25.00	37.00	40.00	41.00	18.00	39.00	39.00	14.50	15.50
V		288		363	383	378	273	462	337	202.00	190.00
Pb					1		1		3	5.9	5.3
REE, ppm											
La	3.90	2.90	4.30	7.42	9.25	9.17	3.03	8.19	9.66	4.00	2.90
Ce	10.70	3.70	8.20	16.67	20.29	19.96	6.18	17.66	21.46	8.30	6.90
Pr				2.31	2.81	2.73	0.83	2.43	2.90	1.31	1.05
Nd	5.70	2.20	6.90	11.64	13.66	13.37	4.44	12.10	14.01	5.90	5.90
Sm	2.90	0.50	3.00	4.07	4.64	4.71	1.67	4.41	4.75	1.71	1.53
Eu	0.90	0.18	1.00	1.43	1.59	1.29	0.70	1.42	1.52	0.49	0.46
Gd				5.14	5.71	5.73	2.31	5.85	6.04	2.08	2.00
Tb	0.60	0.15	0.70	1.02	1.13	1.13	0.46	1.10	1.13	0.41	0.40
Dy				6.78	7.42	7.42	3.12	7.39	7.34	2.54	2.59
Ho				1.47	1.60	1.63	0.70	1.62	1.58	0.57	0.61
Er				4.30	4.59	4.78	2.03	4.58	4.39	1.77	1.84
Tm				0.61	0.65	0.68	0.30	0.67	0.65	0.29	0.31
Yb	3.10	0.96	2.90	3.71	3.94	4.18	1.89	4.09	3.90	1.80	1.90
Lu	0.49	0.16	0.50	0.58	0.63	0.65	0.30	0.63	0.61	0.28	0.32

870

871

872 **Table 6.** Major, trace element and REE data for a selected group of seamount volcanic rocks
 873 from the Ankara Mélange.

Sample no	2007KM327	DM19	KM24	KM27	KM28	KM121	KM126	CM38
Rock-type	Foidite	Trachybasalt	Basanite	Basanite	Trachyte	Tephrrite	Tephryrite	Basanite
Oxide, wt %								
SiO ₂	39.77	50.15	41.08	44.55	68.47	46.36	44.83	44.26
TiO ₂	2.16	2.46	1.64	2.17	0.61	2.10	2.46	2.15
Al ₂ O ₃	15.84	15.90	13.21	15.83	15.16	16.70	15.78	15.75
Fe ₂ O ₃	11.67	9.10	7.75	10.41	3.17	12.04	12.27	10.54
MnO	0.33	0.19	0.12	0.16	0.04	0.18	0.18	0.30
MgO	8.10	3.43	3.91	4.91	0.54	3.12	3.93	9.48
CaO	13.95	5.64	13.78	7.8	1.48	8.59	9.60	4.63
Na ₂ O	0.57	4.74	5.25	4.15	6.79	4.18	3.78	3.98
K ₂ O	1.56	1.91	0.45	2.1	1.35	1.81	1.78	0.74
P ₂ O ₅	0.51	0.77	0.464	0.653	0.484	0.89	0.84	0.68
LOI	5.3	5.5	11.8	7.1	1.7	3.8	4.3	7.1
Total	99.81	99.77	99.46	99.84	99.77	99.73	99.72	99.61
Trace, ppm								
Cr	342.45	13.70	232.87	198.62	13.70	13.70	20.55	219.17
Ni	128.00	21	113	106	20	20	20	130.70
Co	40.10	24.3	30.6	36.4	2.2	26.10	32.50	39.30
Sc	25.00	15	18	20	3	5	7	21
Rb	26.80	39.8	7.7	43.5	33.4	18.7	18.1	13.50
Ba	280	135	151	251	379	426	401	371.00
Sr	223.30	368.6	529.6	588.4	294.3	577.9	547.0	740.00
Cs	0.20	1.00	0.1	1.00	0.7	0.10	0.10	0.30
Th	5.90	7.6	4.9	5.8	10.5	8.8	8.0	6.30
U	1.40	1.6	1.5	1.2	1.4	1.9	1.6	1.60
Nb	55.40	74.5	47.2	60.5	96	88.3	82.0	62.40
Ta	3.00	4.5	2.8	3.6	6	5.1	5.2	3.70
Zr	200.40	291.3	187.2	240	389.5	273.4	257.0	252.10
Hf	4.90	6.9	4.6	6.2	10.2	5.7	5.9	6.50
Y	22.70	24.3	20.6	25	34	29.2	29.0	25.60
V	207	136	157	199	14	90	117	168
Pb	4	1.5	5.6	4.9	7.2	5	7.9	1.8
REE, ppm								
La	37.00	54.4	33	43.4	60.7	63.4	61.1	42.30
Ce	73.00	122.0	64.8	83.5	114.7	128.8	122.9	84.90
Pr	8.80	13.61	7.8	9.71	14.25	13.73	13.57	9.87
Nd	34.30	54.0	29.1	37.3	49	50.7	51.0	39.90
Sm	6.11	9.76	5.21	6.56	8.05	9.06	9.04	6.64
Eu	2.03	3.17	1.74	2.11	2.19	2.84	2.99	2.16
Gd	5.78	8.46	4.65	5.81	6.67	8.33	8.33	6.21
Tb	0.88	1.17	0.76	0.93	1.15	1.18	1.21	0.93
Dy	4.49	5.56	4.01	4.89	6.34	5.88	5.90	4.72
Ho	0.82	0.87	0.76	0.93	1.21	1.07	1.06	0.91
Er	2.11	1.94	2	2.48	3.42	2.72	2.63	2.68
Tm	0.33	0.25	0.29	0.36	0.51	0.36	0.36	0.38
Yb	1.85	1.36	1.71	2.07	3.27	2.18	2.17	2.10
Lu	0.28	0.17	0.25	0.31	0.47	0.30	0.30	0.33

874

875

876 **Table 7.** Major, trace element and REE data for a selected group of island-arc volcanic and
877 syeno-diorite rocks from the Ankara Mélange.

Sample no	04.NAM	05.NAM	06.NAM	DM35	DM 36	DM37	CE960	08CM01	08CM07	KM54
Rock-type	Syeno-diorite	Syeno-diorite	Syeno-diorite	Tephrite	Tephrite	Foidite	Basanite	Leucite Tephrite	Basanite	Basanite
Oxide, wt %										
SiO ₂	50.31	49.35	49.11	41.65	41.86	39.81	42.41	48.29	45.00	46.34
TiO ₂	0.59	0.61	0.62	0.76	0.74	0.70	0.89	0.67	0.79	0.93
Al ₂ O ₃	18.69	18.75	18.39	15.90	15.55	12.84	16.89	18.21	14.57	14.36
Fe ₂ O ₃	8.45	8.77	8.42	10.82	9.31	8.90	12.38	9.15	11.21	11.03
MnO	0.17	0.19	0.19	0.15	0.15	0.14	0.25	0.25	0.21	0.18
MgO	2.25	2.45	2.39	7.23	7.35	10.81	7.5	4.23	6.28	6.33
CaO	6.38	7.14	6.82	3.51	4.08	5.36	11.17	7.91	12.22	9.64
Na ₂ O	2.68	2.57	2.35	0.57	0.46	0.21	2.48	3.78	2.56	2.79
K ₂ O	5.32	5.07	5.68	5.99	6.15	5.15	0.62	2.91	2.15	3.09
P ₂ O ₅	0.48	0.49	0.49	0.44	0.41	0.24	0.42	0.46	0.33	0.44
LOI	4.30	4.20	5.10	12.7	13.6	15.4	4.7	3.7	4.2	4.5
Total	99.61	99.58	99.63	99.69	99.68	99.61	99.71	99.56	99.52	99.67
Trace, ppm										
Cr	47.94	82.19	47.94	13.70	20.55	342.45	21	14.00	130.00	61.64
Ni	20	20	20	23	41	156	43	5.00	24.50	39.00
Co	20.60	22.80	20.70	25.7	28.0	38.4	43.1	24.80	37.10	36.20
Sc	11	11	11	20	21	37	30	20.00	48.00	39.00
Rb	140.2	138.5	148.2	184.1	172.6	162.6	18.3	52.50	29.40	195.80
Ba	1685	1557	1520	783	739	887	577	1883	1051	840
Sr	845.2	915.3	759.4	257.5	331.3	362.2	563.5	742.60	779.80	934.80
Cs	1.1	2.1	3.5	6	4.5	3.4	0.9	3.10	1.20	1.50
Th	11.9	13.9	11.1	10.1	10.3	7.5	4.7	18.00	5.90	5.30
U	3.2	3.1	3.0	3.3	3.7	1.8	1.5	2.40	1.70	2.20
Nb	8.9	9.4	7.6	9.1	8.7	4.2	4	12.30	5.10	3.40
Ta	0.4	0.4	0.3	0.3	0.4	0.1	0.3	0.50	0.20	0.20
Zr	76.1	86.0	72.9	72.8	74.4	49.2	68.9	87.80	57.70	75.20
Hf	1.6	2.2	2.0	2.0	1.7	1.4	2	2.50	1.60	2.00
Y	23.6	23.0	20.3	14.8	16.5	12.5	21.4	20.90	18.70	22.00
V	169	182	166	279	275	260	339	273	301	302
Pb	4	21.8	24.9	3.9	7.4	6.1	5.2	7.3	5.5	9
REE, ppm										
La	33.7	36.6	31.9	26.0	25.7	18.8	20	36.70	20.70	18.40
Ce	60.0	63.7	55.4	53.2	53.5	37.7	42.6	66.70	40.00	41.90
Pr	6.72	7.12	6.20	5.85	5.63	3.93	5.52	7.87	4.89	5.51
Nd	25.3	25.7	24.9	23.0	22.5	15.7	25	32.80	20.70	22.90
Sm	4.91	4.88	4.41	4.42	4.29	3.21	5.27	5.81	4.18	5.12
Eu	1.32	1.31	1.24	1.18	1.21	0.91	1.57	1.53	1.33	1.47
Gd	4.70	4.51	4.18	3.89	4.02	3.21	5.12	5.23	4.31	5.17
Tb	0.70	0.71	0.64	0.57	0.60	0.47	0.79	0.76	0.66	0.80
Dy	3.89	4.11	3.73	2.83	3.28	2.52	4.03	3.88	3.54	4.34
Ho	0.72	0.75	0.67	0.56	0.60	0.46	0.76	0.73	0.69	0.81
Er	2.02	2.14	1.92	1.60	1.61	1.24	2.07	2.05	2.00	2.14
Tm	0.30	0.30	0.28	0.21	0.23	0.17	0.32	0.28	0.29	0.34
Yb	2.16	2.05	1.89	1.49	1.47	1.10	1.82	1.84	1.65	1.94
Lu	0.28	0.33	0.25	0.22	0.23	0.16	0.28	0.27	0.26	0.30
Mg#	35	36	36	57	61	71	55	48	53	53
KO/NaO	1.99	1.97	2.42	10.51	13.37	24.52	0.25	0.77	0.84	1.11

878

879 **Table 8.** Major, trace element and REE data for a selected group of island-arc volcanic rocks from the Ankara Mélange.

Sample no	CE.962	CE.964	CS.07	CS.11	CE.96	CE.98	CS.99	MS.34	MS.35	MS.36	COR.6	COR.7	COR.9	COR.10
Rock-type	Basanite	Basanite	Basanite	Basanite	Basalt	Basalt	Basalt	Basanite	Basanite	Basaltic-trachyandesite	Basanite	Trachy basalt	Trachy basalt	Basanite
Oxide, wt %														
SiO ₂	42.28	42.78	44.35	42.69	51.27	48.78	48.28	44.49	44.56	54.26	44.13	48.08	46.26	42.86
TiO ₂	0.88	0.9	0.78	0.82	0.78	1.74	1.71	1.00	0.92	0.50	0.84	0.84	0.85	0.93
Al ₂ O ₃	16.57	16.84	16.10	16.55	15.91	14.85	14.89	17.60	15.63	17.93	17.26	17.21	18.47	17.03
Fe ₂ O ₃	12.07	12.26	11.44	11.98	9.57	12.69	12.69	9.35	10.31	6.34	9.40	10.17	9.49	10.21
MnO	0.27	0.24	0.21	0.20	0.14	0.20	0.20	0.16	0.19	0.14	0.18	0.19	0.16	0.20
MgO	8	7.37	7.67	6.68	6.44	5.78	5.72	6.82	8.84	2.44	7.21	4.22	4.13	4.74
CaO	10.83	10.42	10.47	9.48	7.64	8.26	8.54	9.17	9.84	5.97	8.84	6.9	8.19	13.37
Na ₂ O	2.7	2.47	3.29	3.88	4.73	3.84	3.48	2.09	2.15	3.75	2.89	4.32	2.35	1.28
K ₂ O	0.73	1.57	0.51	1.06	0.12	0.59	0.75	2.39	2.33	4.10	2.82	2.51	3.01	2.41
P ₂ O ₅	0.38	0.43	0.33	0.39	0.06	0.18	0.16	0.31	0.31	0.27	0.39	0.46	0.34	0.44
LOI	5	4.3	4.5	6.0	3.1	2.7	3.1	6.2	4.5	4	5.6	4.6	6.4	6.1
Total	99.71	99.58	99.65	99.69	99.81	99.57	99.47	99.64	99.61	99.67	99.56	99.48	99.67	99.62
Mg#	57	54	57	52	57	47	47	59	63	43	60	45	46	48
Trace, ppm														
Cr	21	14	68	14	14	41	41	21	82	14	55	14	27	41
Ni	29	37	31.00	19.70	20.40	18.60	18.00	12.20	23.00	5.10	16.7	1.9	15.1	17.5
Co	44.5	43.7	44.10	43.40	31.80	40.10	40.70	33.20	40.60	14.70	32.4	26.5	24.1	40.2
Sc	32	31	41	34	35	37	37	34	49	11	31	15	26	33
Rb	46.5	65.1	11.00	42.50	3.20	8.30	10.00	58.50	55.70	129.20	67.7	38.3	92.4	59.3
Ba	636	2044	596.00	613.00	36.00	882.00	1437.00	796.00	700.00	1225.00	885	2166	902	877
Sr	497.4	620.5	471.90	321.40	43.40	1129.10	1385.20	497.00	460.50	546.70	966.6	875.8	579.5	660.2
Cs	1.3	1	2.90	1.50	32.70	0.70	0.40	2.90	2.70	3.70	4.4	2.1	2.8	2.5
Th	3.8	4.3	3.70	3.90	0.30	0.90	0.90	12.70	11.00	22.90	14.3	12.1	14.3	15.8
U	1	1.2	1.50	1.10	0.10	0.20	0.30	3.20	2.90	5.70	3.6	3	3.1	4.1
Nb	3.1	3.8	4.90	5.40	4.70	7.40	7.10	7.40	6.30	10.30	5.9	6.3	6.4	5.9
Ta	0.2	0.3	2.40	1.60	3.30	3.50	3.90	0.90	1.00	1.50	0.3	0.3	0.4	0.3
Zr	63.3	65	50.60	55.20	46.10	107.30	104.80	110.90	106.30	175.80	126.4	94.4	108.3	113.3
Hf	2.2	1.9	1.50	1.60	1.50	2.90	2.90	2.90	2.90	4.10	3.1	2.6	2.6	2.3
Y	19.6	20.7	18.20	19.80	20.30	34.00	34.10	25.80	24.80	27.10	25.3	24.3	20.4	23.8
V	357	357	365	339	335	379	385	364.00	401.00	157.00	292	282	280	388
Pb	3.6	4.8	5.40	8.30	0.7	0.4	0.6	8.9	8.9	7	13.4	17.5	13.1	18.8

880

881

882 **Table 8. Continued.**

Sample no	CE.962	CE.964	CS.07	CS.11	CE.96	CE.98	CS.99	MS.34	MS.35	MS.36	COR.6	COR.7	COR.9	COR.10
Rock-type	Basanite	Basanite	Basanite	Basanite	Basalt	Basalt	Basalt	Basanite	Basanite	Basaltic-trachyandesite	Basanite	Trachy basalt	Trachy basalt	Basanite
REE, ppm														
La	17.3	17.6	14.90	16.80	3.00	8.40	8.30	37.60	33.30	60.20	43.1	36.2	41.1	43.8
Ce	37.6	39.5	31.60	35.20	7.70	20.90	20.40	73.30	67.00	109.70	90.9	74.4	82.0	92.2
Pr	5.16	5.27	4.16	4.63	1.10	2.90	2.84	8.63	8.13	11.97	9.92	8.46	8.73	9.80
Nd	22.7	23	17.60	20.10	5.20	14.50	13.70	34.50	32.80	43.60	35.3	34.6	31.1	34.8
Sm	4.99	5.22	4.14	4.70	1.86	3.92	3.95	6.88	6.66	7.35	7.23	6.81	5.85	6.93
Eu	1.51	1.53	1.27	1.38	0.74	1.26	1.43	1.94	1.80	1.87	1.96	1.86	1.55	1.79
Gd	4.87	4.94	3.97	4.36	2.49	5.00	5.13	6.21	5.88	5.83	6.42	6	5.30	6.23
Tb	0.72	0.73	0.63	0.70	0.52	0.96	0.97	0.95	0.92	0.90	0.94	0.92	0.76	0.89
Dy	3.92	4.06	3.23	3.47	3.17	5.54	5.76	4.85	4.66	4.68	4.80	4.83	3.66	4.48
Ho	0.71	0.75	0.63	0.68	0.70	1.23	1.23	0.96	0.86	0.91	0.89	0.88	0.76	0.84
Er	1.88	1.96	1.75	1.79	2.17	3.59	3.50	2.46	2.35	2.58	2.44	2.62	2.06	2.28
Tm	0.3	0.31	0.25	0.29	0.33	0.55	0.56	0.39	0.36	0.42	0.35	0.36	0.30	0.34
Yb	1.78	1.78	1.56	1.67	2.11	3.35	3.34	2.38	2.23	2.67	2.27	2.33	1.86	2.19
Lu	0.27	0.27	0.24	0.25	0.33	0.52	0.51	0.36	0.33	0.42	0.35	0.36	0.29	0.33
K ₂ O/Na ₂ O	0.27	0.64	0.16	0.27	0.03	0.15	0.22	1.14	1.08	1.09	0.98	0.58	1.28	1.88

883

884 **Table 9.** Major, trace element and REE data for a selected group of lamprophyric dike rocks from the Ankara Mélange.

Sample no	DM2	DM3	DM4	DM5	DM5A	DM6	DM7	DM7A	DM8	DM9	DM10	DM17	CE1206	CE1207	CE2	CE1210	25BM11
Rock-type	Tephrite	Tephrite	Tephrite	Tephrite	Tephrite	Trachy-basalt	Phono-tephrite	Tephrite	Trachy-basalt	Phono-tephrite	Phono-tephrite	Tephrite	Picro-basalt	Picro-basalt	Picro-basalt	Trachy-basalt	Trachy-andesite
Oxide, wt %																	
SiO ₂	45.25	43.02	47.41	45.84	46.23	48.59	50.29	50.49	49.34	47.48	47.02	46.45	41.94	47.34	44.89	51.33	58.15
TiO ₂	0.69	0.76	0.58	0.64	0.66	0.73	0.62	0.62	0.70	0.73	0.74	0.78	1.12	0.83	1.26	1.24	0.43
Al ₂ O ₃	11.20	10.93	15.79	16.98	17.00	10.34	14.94	14.73	12.10	14.37	14.66	11.40	12.91	15.66	13.36	15.62	17.43
Fe ₂ O ₃	11.16	12.10	9.54	10.86	11.03	11.46	10.85	10.72	10.92	11.07	11.13	12.59	10.8	9.79	11.12	7.33	5.81
MnO	0.23	0.22	0.23	0.21	0.21	0.22	0.20	0.18	0.21	0.24	0.23	0.22	0.2	0.21	0.22	0.08	0.14
MgO	5.41	4.98	2.90	4.66	4.87	6.02	4.02	4.13	4.49	3.43	3.50	5.09	7.71	4.02	8.23	5.99	1.88
CaO	14.50	15.89	12.25	10.25	9.57	13.68	7.30	7.53	13.50	8.44	8.53	12.26	16.47	9.11	14.37	8.22	4.04
Na ₂ O	0.67	0.28	0.36	1.63	1.68	0.56	2.84	2.78	1.96	2.64	2.95	1.58	1.62	2.97	1.70	3.95	5.56
K ₂ O	5.47	5.54	6.96	4.67	4.99	5.73	5.53	5.50	4.11	6.34	5.82	5.40	0.72	4.5	1.01	1.85	4.32
P ₂ O ₅	0.89	0.80	0.45	0.44	0.40	1.08	0.96	0.93	0.89	0.78	0.78	0.90	0.49	0.64	0.55	0.75	0.29
LOI	4	4.9	2.9	3.4	3.0	1.1	2.0	1.9	1.3	3.7	3.9	2.8	5.8	4.6	2.9	3.4	1.6
Total	99.5	99.46	99.42	99.61	99.60	99.49	99.53	99.53	99.52	99.27	99.28	99.48	99.78	99.67	99.64	99.76	99.64
Trace, ppm																	
Cr	13.70	13.70	13.70	13.70	13.70	13.70	13.70	13.70	13.70	13.70	13.70	13.70	89	21	82	158	68
Ni	20	20	20	20	20	20	20	20	20	20	20	20	48	28	67	86	45
Co	33.0	39.4	26.9	34.8	34.5	37.9	34.1	33.8	32.2	28.5	28.9	41.2	35.5	24.2	39.7	24.9	12.50
Sc	30	34	10	25	27	45	24	25	30	21	22	36	41	22	39	19	7
Rb	51.4	52.6	94.6	76.9	81.5	46.9	65.0	67.7	29.7	47.3	43.1	50.0	20.8	75.5	13.8	29.9	76.5
Ba	1861	1881	2899	1224	1228	1760	1183	1233	1846	3229	3172	2019	180	1109	257	475	1456
Sr	697.0	864.1	762.5	701.6	811.3	823.9	1483.3	1401.6	758.9	1287.1	1335.2	790.0	1073	1116	805.4	1006	679.1
Cs	0.1	0.1	0.2	0.3	0.2	0.1	0.1	0.1	0.1	0.4	0.4	0.1	0.3	0.6	0.1	0.2	0.1
Th	24.4	14.0	19.7	8.9	9.1	21.9	14.2	14.4	23.1	34.6	33.6	13.2	7.3	14.9	6.9	5.4	25.0
U	6.0	5.6	7.4	2.9	3.1	5.4	7.1	6.9	6.0	10.1	10.5	5.1	2.4	4.9	2.5	1.0	6.9
Nb	18.3	22.7	18.4	7.8	7.9	17.0	13.7	13.9	18.6	34.1	33.9	21.7	9.7	13.1	15.1	7.4	10.7
Ta	0.6	0.7	0.7	0.3	0.3	0.7	0.5	0.5	0.6	1.1	1.2	0.7	0.6	0.9	1.0	1	0.6
Zr	111.4	111.2	117.3	65.0	62.3	103.2	95.1	93.8	112.6	188.1	186.3	101.6	92.9	163.5	111.9	121.9	199.7
Hf	2.8	2.9	2.8	1.6	1.4	2.7	2.5	2.3	2.8	4.7	4.4	2.6	2.5	4.1	2.8	3.1	4.3
Y	23.7	24.5	22.1	16.2	15.1	24.4	21.5	20.4	24.8	34.2	34.4	23.7	21.9	34.8	24.7	16.9	28.9
V	305	403	405	307	299	329	262	269	347	329	329	370	300	245	330	162	116
Pb	32.3	17.0	11.1	16.8	15.5	14.8	9.6	8.8	9.4	12.6	11.3	20.2	2.3	6.6	0.9	1.30	33.9
Mg#	49	45	38	46	47	51	42	43	45	38	38	44	59	45	59	62	39
KO/NaO	8.16	19.79	19.33	2.87	2.97	10.23	1.95	1.98	2.10	2.40	1.97	3.42	0.44	1.52	0.59	0.47	0.78

885

886 **Table 9. Continued.**

Sample no	DM2	DM3	DM4	DM5	DM5A	DM6	DM7	DM7A	DM8	DM9	DM10	DM17	CE1206	CE1207	CE2	CE1210	25BM11
Rock-type	Tephrite	Tephrite	Tephrite	Tephrite	Tephrite	Trachy- basalt	Phono tephrite	Tephrite	Trachy- basalt	Phono tephrite	Phono tephrite	Tephrite	Picro- basalt	Picro- basalt	Picro- basalt	Trachy- basalt	Trachy- andesite
REE, ppm																	
La	60.0	41.8	49.5	26.4	25.0	56.6	32.2	30.7	58.4	83.6	81.2	41.4	26.3	43.2	29.3	33.3	69.2
Ce	120.4	87.4	97.8	52.4	49.7	115.9	69.8	67.3	119.6	159.0	156.7	86.5	53.1	88.9	58.1	70.7	124.9
Pr	13.07	9.79	10.41	5.75	5.52	13.12	7.99	7.71	13.19	16.87	16.92	9.76	6.83	10.9	7.52	8.76	13.24
Nd	49.9	39.3	38.7	22.2	22.3	53.9	32.7	32.0	51.5	63.2	63.9	39.6	28.2	42.5	29.8	33.1	46.9
Sm	9.36	8.07	7.17	4.49	4.29	9.83	6.15	5.93	9.48	11.52	11.64	7.84	5.98	8.52	6.96	5.67	7.82
Eu	2.26	2.02	1.86	1.20	1.14	2.35	1.53	1.50	2.27	2.84	2.88	2.00	1.72	2.49	1.98	1.59	1.93
Gd	7.94	7.09	6.23	4.01	3.88	8.37	5.32	5.22	7.97	10.04	10.03	7.19	5.68	8.09	6.36	4.56	6.22
Tb	1.04	0.97	0.88	0.59	0.56	1.07	0.77	0.76	1.07	1.36	1.36	0.95	0.86	1.21	0.93	0.67	0.90
Dy	4.95	4.71	4.31	2.95	2.97	4.94	3.94	3.91	4.88	6.88	6.66	4.72	4.06	6.33	4.68	3.28	4.98
Ho	0.82	0.82	0.73	0.55	0.55	0.79	0.74	0.73	0.84	1.16	1.19	0.80	0.79	1.2	0.81	0.61	0.91
Er	2.05	2.12	2.00	1.50	1.45	2.10	1.96	1.94	2.08	3.08	3.02	2.10	2.09	3.27	2.30	1.64	2.63
Tm	0.29	0.29	0.27	0.22	0.21	0.28	0.29	0.27	0.29	0.43	0.44	0.30	0.32	0.52	0.33	0.25	0.42
Yb	1.65	1.79	1.83	1.41	1.33	1.69	1.74	1.76	1.69	2.67	2.80	1.73	1.76	2.94	1.89	1.47	2.66
Lu	0.25	0.27	0.26	0.21	0.20	0.25	0.27	0.26	0.25	0.41	0.41	0.26	0.27	0.46	0.27	0.22	0.43
⁸⁷ Sr/ ⁸⁶ Sr		0.704786			0.704892			0.704697	0.704720			0.704797			0.704820		
¹⁴³ Nd/ ¹⁴⁴ Nd		0.512681			0.512686			0.512690	0.512682			0.512680			0.512674		
²⁰⁶ Pb/ ²⁰⁴ Pb		19.540			19.332			19.939	19.604			19.594			19.418		
²⁰⁷ Pb/ ²⁰⁴ Pb		15.662			15.655			15.691	15.675			15.659			15.664		
²⁰⁸ Pb/ ²⁰⁴ Pb		39.376			39.192			39.612	39.536			39.407			39.297		

887